Cell

Pangenome-guided breeding restores high-altitude adaptation and improves yield in Tartary buckwheat

Graphical abstract

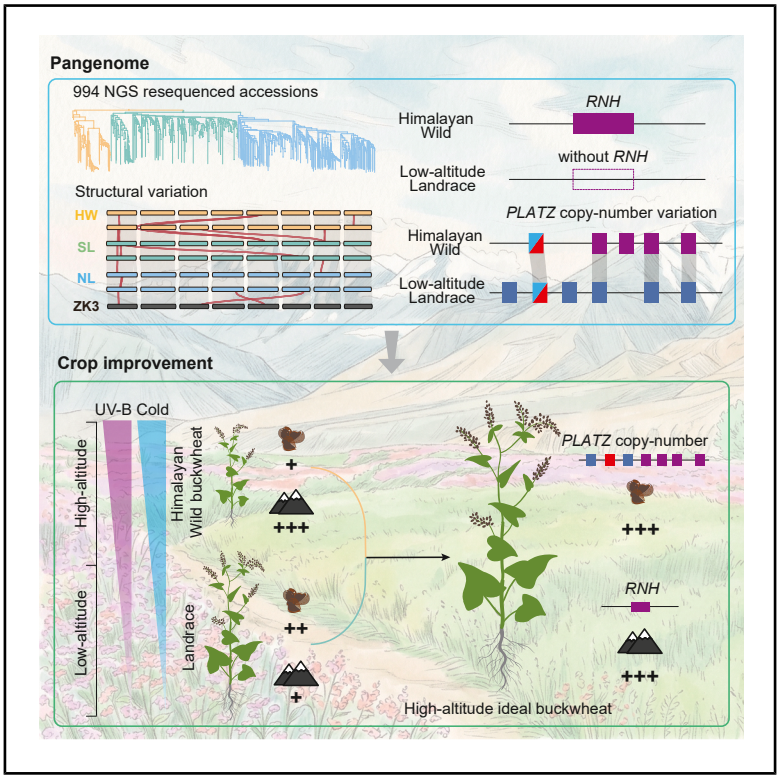

Highlights

- Structural variations are diverse between wild buckwheat and landraces
- The presence of *FtRNH* in wild accessions is associated with high-altitude adaptability
- Structural variations in *FtPLATZ* are linked to seed-size variations
- An ideal highland buckwheat is developed by integrating superior alleles

Authors

Kaixuan Zhang, Yuqi He, Hao Lin, ..., Rajeev K. Varshney, Jianquan Liu, Meiliang Zhou

Correspondence

heyuqi@caas.cn (Y.H.), liuxu03@caas.cn (X.L.), rajeev.varshney@murdoch.edu.au (R.K.V.), liujq@nwipb.cas.cn (J.L.), zhoumeiliang@caas.cn (M.Z.)

In brief

A Tartary buckwheat pangenome is constructed, allowing identification of the wild-specific gene *FtRNH* conferring high-altitude adaptation, as well as *FtPLATZ* structural variants controlling seed size. By combining these superior alleles, buckwheat lines are developed with enhanced high-altitude adaptability and improved field yields.

Zhang et al., 2026, Cell *189*, 1–18

https://doi.org/10.1016/j.cell.2026.07.035

CellPress

Please cite this article in press as: Zhang et al., Pangenome-guided breeding restores high-altitude adaptation and improves yield in Tartary buckwheat, Cell (2026), https://doi.org/10.1016/j.cell.2026.07.035

Cell

CellPress

Article

Pangenome-guided breeding restores high-altitude adaptation and improves yield in Tartary buckwheat

Kaixuan Zhang,[1,23] Yuqi He,[1,23,*] Hao Lin,[2,1,23] Jiayue He,[1,23] Zhirong Wang,[1,23] Wei Li,[1,23] Yanhua Chen,[1,23] Jing Li,[3,4,23] Yaliang Shi,[1] Xu Huang,[1] Mengqi Ding,[5] Pu Yang,[4] Zhiqiang Chen,[6] Annapurna Chitikineni,[7] Jiguang Li,[8] Jinfeng Gao,[4] Baili Feng,[4] Zongwen Zhang,[9] Ming Hao,[10] Reyazul Rouf Mir,[7] Dengcai Liu,[10] Sun-Hee Woo,[11] Dagmar Janovská,[12]

(Author list continued on next page)

[1]State Key Laboratory of Crop Gene Resources and Breeding, Key Laboratory of Grain Crop Genetic Resources Evaluation and Utilization (MARA), National Key Facility for Crop Gene Resources and Genetic Improvement, Institute of Crop Sciences, Chinese Academy of Agricultural Sciences, Beijing 100081, China
[2]Sichuan Zoige Alpine Wetland Ecosystem National Observation and Research Station, Key Laboratory for Bio-Resource and Eco-Environment of Ministry of Education, College of Life Science, Sichuan University, Chengdu 610065, China
[3]School of Life Sciences, Shaanxi Key Laboratory of Chinese Jujube, Yan'an University, Yan'an 716000, Shaanxi, China
[4]College of Agronomy, State Key Laboratory for Crop Stress Resistance and High-Efficiency Production, Northwest A and F University, Yangling 712100, Shaanxi, China
[5]College of Agronomy and Biotechnology, Southwest University, Chongqing 400715, China
[6]Beijing Glbizzia Biotechnology Co., Ltd, Beijing 102629, China
[7]Centre for Crop and Food Innovation, WA State Agricultural Biotechnology Centre, Food Futures Institute, Murdoch University, Murdoch, Perth, WA 6150, Australia
[8]Crop Research Institute, Hunan Academy of Agricultural Sciences, Changsha 410125, Hunan, China
[9]Alliance of Bioversity International and CIAT, Via di San Domenico 100153 Rome, Italy
[10]Triticeae Research Institute, Sichuan Agricultural University, Chengdu 611130, China
[11]Department of Crop Science, Chungbuk National University, Cheong-ju 28644, South Korea
[12]Gene Bank, Czech Agrifood Research Center (former Crop Research Institute), Drnovská 507/73, Prague 6-Ruzyně, Prague 161 06, Czechia
[13]Groupe de Recherche en Physiologie Végétale (GRPV), Earth and Life Institute-Agronomy (ELI-A), Université Catholique de Louvain, Croix du Sud 45, boîte L7.07.13, Louvain-la-Neuve B-1348, Belgium
[14]Department of Root Biology and Symbiosis, Max-Planck-Institute of Molecular Plant Physiology, 14476 Potsdam, Germany
[15]Xizang Academy of Agriculture and Animal Husbandry Sciences, Jinzhu West Road 130, Lhasa 850000, Xizang Autonomous Region, China
[16]Xizang Agricultural and Animal Husbandry University, Yucai West Road 100, Linzhi 860000, Bayi District, Xizang Autonomous Region, China
[17]Department of Biotechnology, School of Science, Kathmandu University, PO Box 6250, Dhulikhel 45200, Nepal
[18]School of Health and Allied Sciences, Pokhara University, Pokhara 30, Dhungepatan, Pokhara, Gandaki 33700, Nepal
[19]Nutrition Institute, Koprska Ulica 98, SI-1000 Ljubljana, Slovenia

(Affiliations continued on next page)

SUMMARY

Tartary buckwheat is a nutritionally important crop of the Himalayas and is crucial for local economies and food security. However, key genes and superior alleles for high-altitude adaptability and yield remain poorly defined, constraining the breeding of high-altitude buckwheat varieties. Here, we generated a telomere-to-telomere reference genome and a 16-accession pangenome spanning Himalayan wild populations and globally distributed landraces. We identified 123,131 non-redundant structural variations in 16 accessions, including gene copy-number variations. The graph-based pangenome revealed *FtRNH*, a wild-specific gene that enhances high-altitude adaptability. We also identified a copy-number variation at the *FtPLATZ* locus and a 28-bp insertion in the *FtPLATZ3* promoter that together contribute to seed-size variation across wild buckwheat and landraces. Leveraging these superior *FtRNH* and *FtPLATZ* alleles, we developed buckwheat lines with enhanced high-altitude adaptability and improved yields across sites. These findings establish a pangenome-guided strategy for recovering wild alleles and combining stress adaptation with yield improvement in crops.

INTRODUCTION

As the highest-altitude region in the world, the Himalayan region encompassing Nepal, Bhutan, southern Xizang of China, northern India, and northeastern Pakistan faces severe food security challenges.[1] Achieving the United Nations Sustainable Development Goals (SDGs) of zero hunger necessitates enhancing food and nutrition security and promoting the marketization of local

Muriel Quinet,[13] Alisdair R. Fernie,[14] Wenhua Liao,[15] Xibo Feng,[16] Dhurva Prasad Gauchan,[17] Namraj Dhami,[18] Ivan Kreft,[19] Artur Piński,[20] Alexander Betekhtin,[20] Manuel Spannagl,[21] Xu Liu,[1,*] Rajeev K. Varshney,[7,*] Jianquan Liu,[22,2,*] and Meiliang Zhou[1,24,*]

[20]Institute of Biology, Biotechnology, and Environmental Protection, Faculty of Natural Sciences, University of Silesia in Katowice, Katowice 40-007, Poland
[21]Plant Genome and Systems Biology, German Research Center for Environmental Health, Helmholtz Zentrum München, Neuherberg 85764, Germany
[22]State Key Laboratory of Herbage Improvement and Grassland Agro-ecosystems, College of Ecology, Lanzhou University, Lanzhou 730000, China
[23]These authors contributed equally
[24]Lead contact
*Correspondence: heyuqi@caas.cn (Y.H.), liuxu03@caas.cn (X.L.), rajeev.varshney@murdoch.edu.au (R.K.V.), liujq@nwipb.cas.cn (J.L.), zhoumeiliang@caas.cn (M.Z.)
https://doi.org/10.1016/j.cell.2026.07.035

crops. However, intense ultraviolet B (UV-B) radiation and low temperature in the Himalayas make it impossible for most economically valuable crops to survive. One notable crop that both originated and is widely cultivated in this area is Tartary buckwheat (*Fagopyrum tataricum*, Polygonaceae),[2–4] while barley, another major crop in the Himalayas, originated in the Fertile Crescent.[5]

Tartary buckwheat is a traditional underutilized crop, commonly used as a food and forage crop in high-altitude regions[4,6] (Figure S1A). It is gaining popularity worldwide for its rich bioactive compounds, which are consumed as tea or nutritional supplements or processed into wine. Among these compounds, flavonoids are particularly significant, having been extensively studied for their health benefits.[6–8] The enhanced flavonoid content also provides greater resistance to UV-B radiation and cold stress.[9–11] Despite the rich germplasm shaped by long-term selection,[12] buckwheat cultivated in the Himalayas primarily relies on old landraces with small seeds and low yields,[2,3,13] while low-altitude landraces developed through artificial selection for large seeds have partially compensated for this yield deficiency.[2,3] However, all cultivated landraces, including those cultivated in the Himalayas, exhibit weaker high-altitude adaptation than wild accessions of the same region.[3] Furthermore, the genetic mechanisms controlling seed traits and high-altitude adaptability remain unclear, hindering progress in the molecular breeding of highland crops.

Recent advances in genome sequencing have facilitated the discovery of the genetic basis for agronomic traits in Tartary buckwheat. For example, whole-genome resequencing and comparative genomics have revealed the population structure and genetic variation underlying agronomic traits,[2,3] flavonoid content,[13–15] and environmental adaptation[2,16] in germplasm. However, existing data are insufficient, as current genomes contain substantial gaps and are limited to a few landraces, representing only a fraction of total genetic diversity,[2,14,17] and short-read sequencing complicates identification of large structural variations[2,3] (SVs, $\geq$20 bp), including gene copy-number variations (CNVs). Pangenomes offer a solution by facilitating identification of large-scale SVs associated with agronomic traits and environmental adaptation,[18,19] particularly beneficial genes or alleles in wild accessions lost during domestication.[20] Hence, generating a graph-based pangenome by integrating high-quality genomes from comprehensive germplasm is crucial.

To achieve a comprehensive understanding of the genetic underpinnings of phenotypic variation, we report a telomere-to-telomere (T2T) reference genome of Tartary buckwheat, along with a pangenome encompassing Himalayan wild accessions and global landraces. By integrating high-resolution variation maps from 994 accessions, we generated a graph-based genome enabling the identification of large-scale SVs, including gene presence/absence and variable gene copy number, which underlie differences in agronomic traits and environmental adaptability. Leveraging these SVs, we selected specific germplasms with enhanced yield or high-altitude adaptability for breeding an ideal buckwheat variety. These results will help bridge gaps in high-altitude crop breeding and provide scientific support for improving crop yield in the Himalayan region.

RESULTS

The T2T reference genome and population genetic structure of the global accessions

To provide a complete reference genome for exploring population genomic variation, a widely adapted and cultivated Tartary buckwheat variety ZK3 (ZHONGKU NO. 3; Figure 1A), known for its tall plant height and high yield, was selected for T2T genome assembly using PacBio high-fidelity (HiFi) and Oxford Nanopore Technologies (ONT) sequencing platforms. Using 31.5 Gb HiFi reads and 16.7 Gb ultra-long reads, a T2T genome with an N50 of 56.7 Mb was assembled (Figures S1B and S1C; Tables S1A and S1B). The eight longest contigs, encompassing 453.6 Mb, aligned well with the known chromosome-level genome (Figure S1D). Benchmarking universal single-copy orthologs (BUSCO) analysis identified 98.5% of core conserved genes (Table S1B). A total of 28,531 genes were annotated (Table S1C). Moreover, 97.6% (1,575 out of 1,614) of core conserved plant genes were fully identified using BUSCO analysis, indicating the credibility of our ZK3 gene annotations (Table S1D). This assembly exhibited high collinearity and filled 31 gaps harboring 48 new genes (Figures S1C and S1D; Table S1E) compared to the Pinku genome that is widely used for genomic analysis, RNA-seq, and gene family analysis.[16,21,22] We identified 16 telomeres and 8 putative centromeres on the 8 chromosomes (Tables S1F and S1G). The conserved telomeric repeat units $(CCGAAA)_n$ and $(CCTGAA)_n$ match the sequence reported for this species.[23] Centromere positions were verified

Please cite this article in press as: Zhang et al., Pangenome-guided breeding restores high-altitude adaptation and improves yield in Tartary buckwheat, Cell (2026), https://doi.org/10.1016/j.cell.2026.07.035

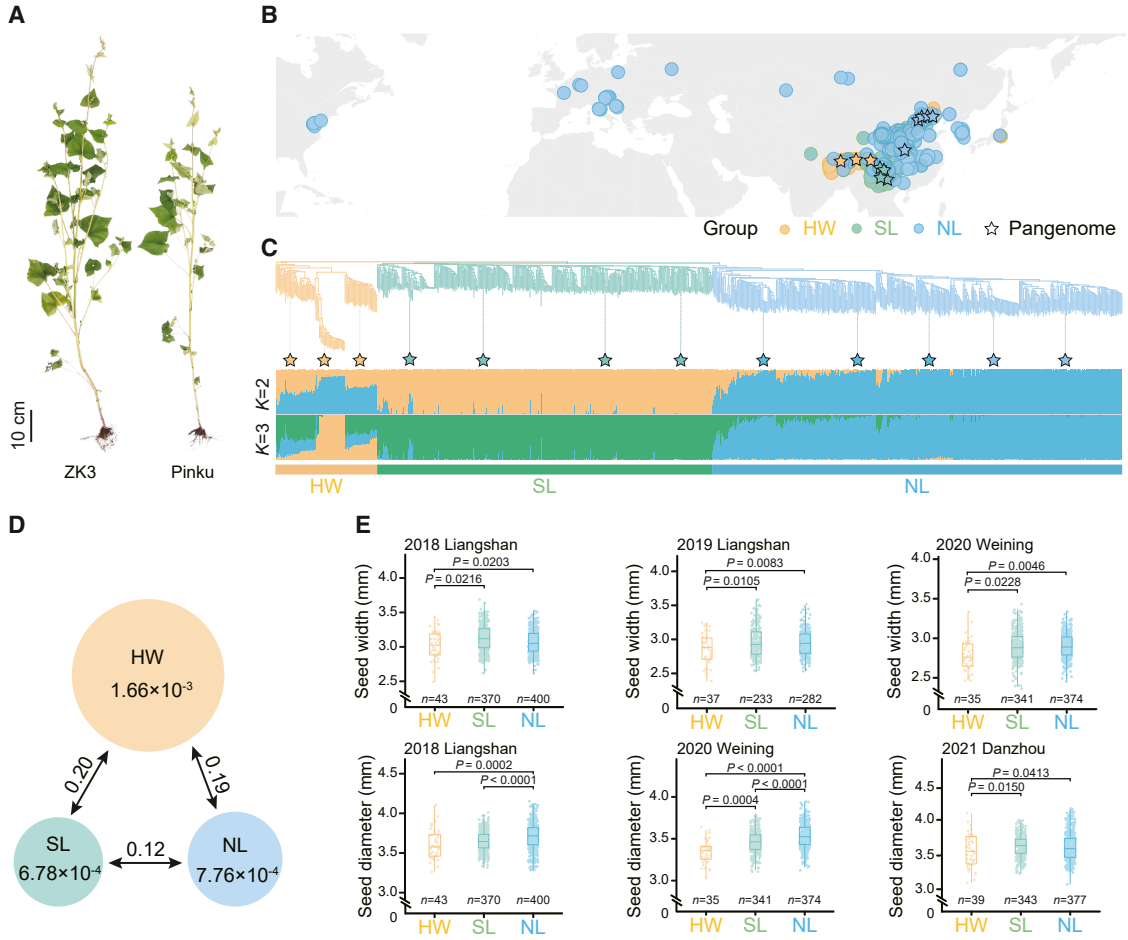

Figure 1. Population structure and phenotypic variation among Tartary buckwheat germplasms

(A) Phenotypes of the ZK3 and Pinku varieties at 70 days after germination under the same ecological conditions in Zhaotong.

(B) Geographic distribution of the 994 accessions used in this study. HW, Himalayan wild group; SL, Southwestern landraces group; NL, Northern landraces group.

(C) Phylogenetic tree and population structure of 994 Tartary buckwheat accessions, with inferred clusters at $K = 2$ and $K = 3$.

(D) Genomic diversity (π, within circles) and pairwise fixation index (F_{ST}, between circles) among three genetic groups. Circle size is proportional to π.

(E) Seed width and diameter differences among HW, SL, and NL groups across multiple environments and years. Significance was assessed by one-way ANOVA with exact p values shown.

through chromatin immunoprecipitation sequencing (ChIP-seq) using a centromeric histone H3 (CENH3) antibody (Figures S1E and S1F) and fluorescent probe hybridization (Figure S1G). The concordance of our assembly with experimental data at centromeres, which are challenging to assemble due to their repetitive nature, orthogonally validates its continuity and completeness.

Although the genetic structure of Tartary buckwheat germplasms has been constructed,[2,3] harsh environments led to insufficient collection of Himalayan accessions. To this end, we integrated 35 newly collected wild accessions from the Himalayas and 379 landraces from around the world, including the Himalayas, for genome resequencing. With prior data, we obtained a dataset of 994 accessions from 15 countries, with an average depth >16× covering 98.3% of the genome (Figures 1B and 1C; Table S1H). This collection had a wider altitude distribution and larger phenotypic variation (Figure S1H). Using the ZK3-T2T reference, we identified 25,158,039 high-quality SNPs and 134,702 insertions or deletions (indels) (Table S1I). Phylogenetic and population structure analysis (Figure 1C; Figure S1I) illustrated three groups (Himalayan wild group, HW; Southwestern landraces group, SL; and Northern landraces group, NL) consistent with previous classifications.[2,3] Among newly added accessions, 176 local landraces mainly from northern China and the high-altitude Himalayan region were grouped into NL, 197 accessions mainly from southern China and the Himalayan region were grouped into SL, and 41 accessions from the Himalayan region were grouped into HW, which mainly comprises wild accessions and a few Himalayan landraces.

We further examined genetic diversity among the three groups. Genomic diversity was higher in HW ($\pi_{HW} = 1.66 \times 10^{-3}$), which includes all wild accessions, than in SL ($\pi_{SL} = 6.78 \times 10^{-4}$) and NL ($\pi_{NL} = 7.76 \times 10^{-4}$), which include only cultivated accessions

Please cite this article in press as: Zhang et al., Pangenome-guided breeding restores high-altitude adaptation and improves yield in Tartary buckwheat, Cell (2026), https://doi.org/10.1016/j.cell.2026.07.035

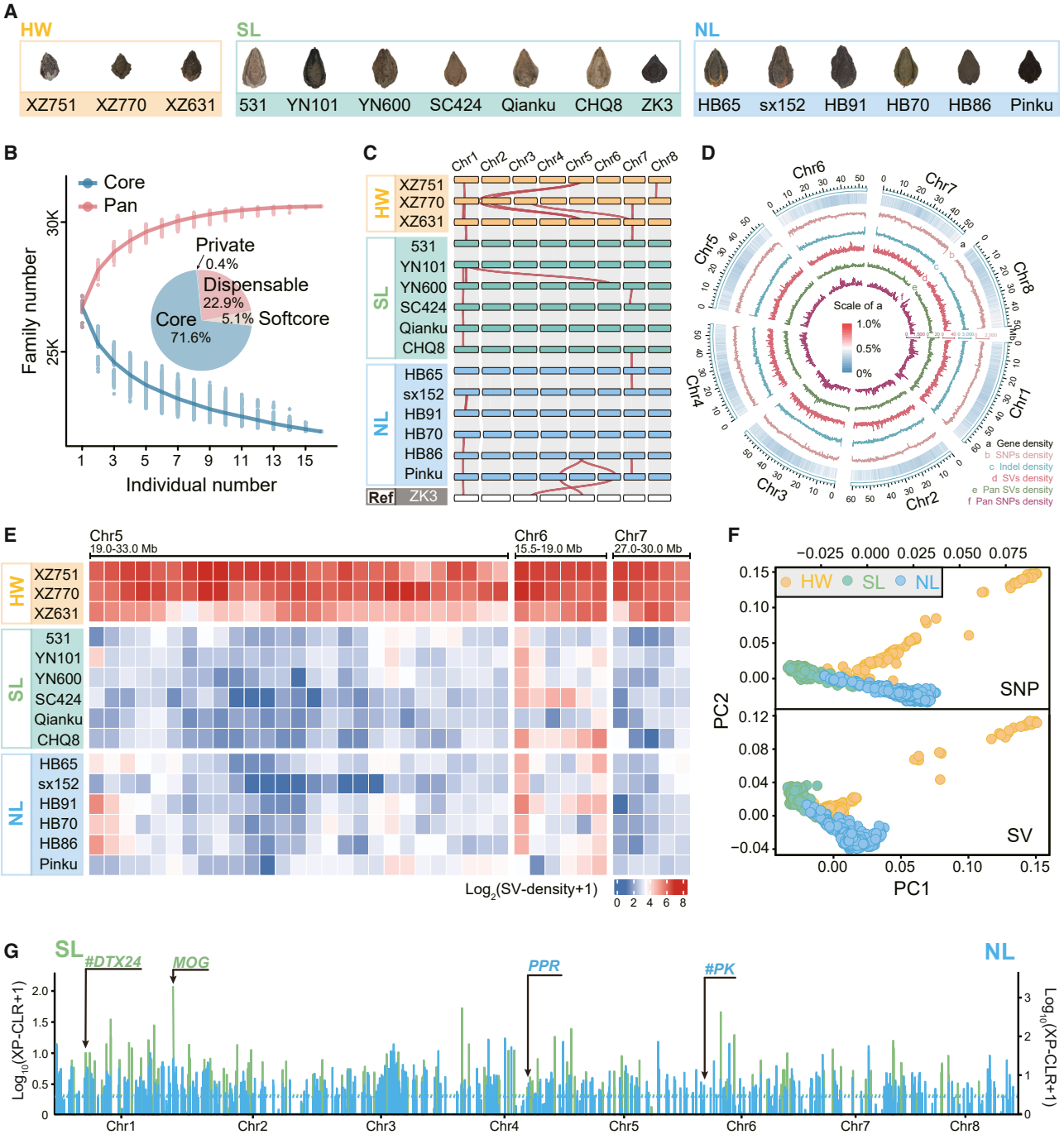

Figure 2. Genomic SVs revealed by the Tartary buckwheat pangenome

(A) Seed morphology of representative wild accessions and landraces used for genome assembly.

(B) Gene family dynamics in the pangenome. The line plot represents the number of core and pan gene families as the number of included genomes increases. The pie chart represents proportions of specific gene families.

(C) Synteny and inversions across eight chromosomes in 16 Tartary buckwheat genomes. Grey lines represent conserved synteny blocks, and red lines represent inversions.

(D) Circular visualization of density of genomic features in the graph-based pangenome. From outer to inner: a, gene; b, SNP (vs. ZK3-T2T); c, indel (vs. ZK3-T2T); d, SV (vs. ZK3-T2T); e, SV (vs. graph-based pangenome); f, SNP (vs. graph-based pangenome).

(E) SV counts in three SV hotspot regions across 15 genomes. Colors represent SV numbers per 1 Mb window (0.5 Mb step).

(legend continued on next page)

Please cite this article in press as: Zhang et al., Pangenome-guided breeding restores high-altitude adaptation and improves yield in Tartary buckwheat, Cell (2026), https://doi.org/10.1016/j.cell.2026.07.035

(Figure 1D). This confirms the Himalayan region as the center of origin and genetic diversity of Tartary buckwheat because cultivated landraces fall within all three groups, while HW (containing wild accessions) exhibits the highest genetic diversity. Linkage disequilibrium (LD) decayed faster in HW (comprising wild accessions) than in SL and NL (containing only cultivated accessions) (Figure S1J). The pairwise fixation index (F_{ST}) between HW and the two cultivated groups was 1.67 and 1.58 times higher than that between SL and NL (Figure 1D). We also observed significant differences in yield-related agronomic traits (e.g., seed width and diameter) between wild accessions and landraces (Figure 1E).

Pangenome construction and genomic variations of all sampled accessions

To explore the genomic variations responsible for agronomic trait variation in Tartary buckwheat germplasms, three HW, four SL, and five NL accessions were selected for genome assembly based on phylogenetic relationship and geographic distribution (Figures 1C and 2A; Figure S2A; Tables S2A and S2B). All 12 genomes reached reference-quality assembly standards, with a long terminal repeat (LTR) assembly index (LAI) $\geq$10 and BUSCO completeness >96.6%. Combining the ZK3-T2T, three previously published genomes,[2,14,17] and 12 newly assembled genomes, we established a pangenome of 16 assemblies (Table S2B). These genomes exhibited little difference in genome size (450.20–459.10 Mb), gene number (28,531–29,685), and repeat sequence proportion (50.98%–52.92% of the genome size; Tables S2B and S2C).

Using these 16 genomes, we constructed the pangenome of Tartary buckwheat and identified 30,604 gene families, with pan gene families plateauing when the genome count exceeded 13 (Figure 2B), indicating the representativeness of these accessions. These gene families were defined as core (71.6%), softcore (5.1%), dispensable (22.9%), and private (0.4%) (Figure 2B; Tables S2D–S2G). Genes in core families exhibited longer lengths, lower exon length ratios, and fewer non-synonymous mutations, compared with other categories (Figures S2B–S2D), indicating their conservation. Additionally, the proportion of core and softcore genes containing Pfam domains was higher than that of private genes (Figure S2E). Kyoto Encyclopedia of Genes and Genomes (KEGG) analysis revealed that genes in core and softcore gene families were mainly enriched in primary metabolism (e.g., amino acid, nucleotide, and lipid metabolism), while non-core genes were enriched in secondary metabolism (e.g., flavonoid biosynthesis and hormone signaling; Table S2H). We identified 3,996 gene families absent in ZK3-T2T (Figure S2F), suggesting that this pangenome compensates for the limited genetic diversity coverage of a single reference genome. Pangenome analysis also identified eight large-scale inversions distributed across chromosomes (Figure 2C; Table S2I).

We further performed SV (including gene CNVs) calling across 15 genomes using ZK3-T2T as a reference to construct a graph-based pangenome. A total of 123,131 non-redundant SVs ($\geq$20 bp) were identified, comprising 46.64% presences, 51.62% absences, 1.52% translocations, and 0.22% inversions (Figure 2D; Table S2J). Most SVs were <2 Kb and distributed in intergenic regions (Figure S2G; Tables S2J and S2K). Based on frequency across 15 genomes, SVs were further classified into core (present in all 15), softcore (present in >90% but not all), dispensable (present in >1% but <90%), and private (present in only one) categories (Figure S2H). Presence and absence variations (PAVs) accounted for the majority of SVs in each genome (Figure S2I). Additionally, we identified SV hotspots on chromosomes 5, 6, and 7, where HW accessions harbored more SVs than SL and NL (Figure 2E; Table S2L). These SV-enriched regions, specific to wild Tartary buckwheat, may harbor regulatory variants underlying adaptation traits.

In order to identify SVs responsible for differences in agronomic and adaptability traits, we mapped the resequencing data to the graph-based pangenome and verified them using PCR (Table S2M). SV-based principal-component analysis (PCA) revealed three divergent groups consistent with those based on SNPs identified using ZK3-T2T as the reference (Figure 2F; Figure S2J). We further screened genes under selection based on SNPs identified using ZK3-T2T as the reference (283 sweeps, 2,133 genes in HW vs SL; 276 sweeps, 2,020 genes in HW vs NL) and SVs identified using a graph-based pangenome as the reference (130 sweeps, 818 genes in HW vs SL; 314 sweeps, 2,251 genes in HW vs NL) through the cross-population composite likelihood ratio test (XP-CLR; Figure 2G; Tables S2N–S2Q). A total of 254 genes overlapped between SNP- and SV-based analyses (Tables S2P–S2Q), with 72 genes overlapping previously reported selection regions using SNPs[2,3] (Figure 2G; Figure S2K). We further analyzed whether SV-based selective sweeps overlapped with previous genome-wide association study (GWAS) results[13] and found 1,667 genes associated with 292 metabolites within these sweeps (Tables S2P and S2Q). We also recovered more SVs within or near these genes (Figure S2L), which may serve as targets of natural or artificial selection and valuable markers for molecular breeding.

The unique presence and likely high-altitude adaptability role of *FtRNH* in Himalayan wild accessions

The Himalayan wild accessions XZ751 and XZ770 (HW group), which inhabit higher altitudes than all cultivated landraces, exhibited a greater number of private gene families (Table S2G) and private SVs (Figure S2H). To identify SVs (including PAVs and CNVs) associated with high-altitude adaptability, we used the genome of XZ751 (which grows at a higher altitude than XZ770) as the reference for SV identification across all sampled genomes (Figure S2M). A total of 218 absent SVs were identified in the other 14 genomes compared with XZ751 and XZ770 (Table S3A). Notably, five PAVs resulted in six private genes specific to XZ751 and XZ770 (Table S3B). Among these, one gene encoding a ribonuclease H protein (*FtRNH*; Figure S2N;

(F) PCA of 994 Tartary buckwheat accessions based on SNPs (upper) and SVs (lower), using PC1 and PC2.

(G) Genomic regions under selection in SL (green) and NL (blue) relative to HW, identified by SV-based XP-CLR (top 5% threshold). Genes marked "#" harbor SVs associated with metabolite content divergence between wild accessions and landraces. Unmarked genes were identified in both SNP- and SV-based XP-CLR analyses, with additional new SVs identified specifically in the SV-based scan.

Please cite this article in press as: Zhang et al., Pangenome-guided breeding restores high-altitude adaptation and improves yield in Tartary buckwheat, Cell (2026), https://doi.org/10.1016/j.cell.2026.07.035

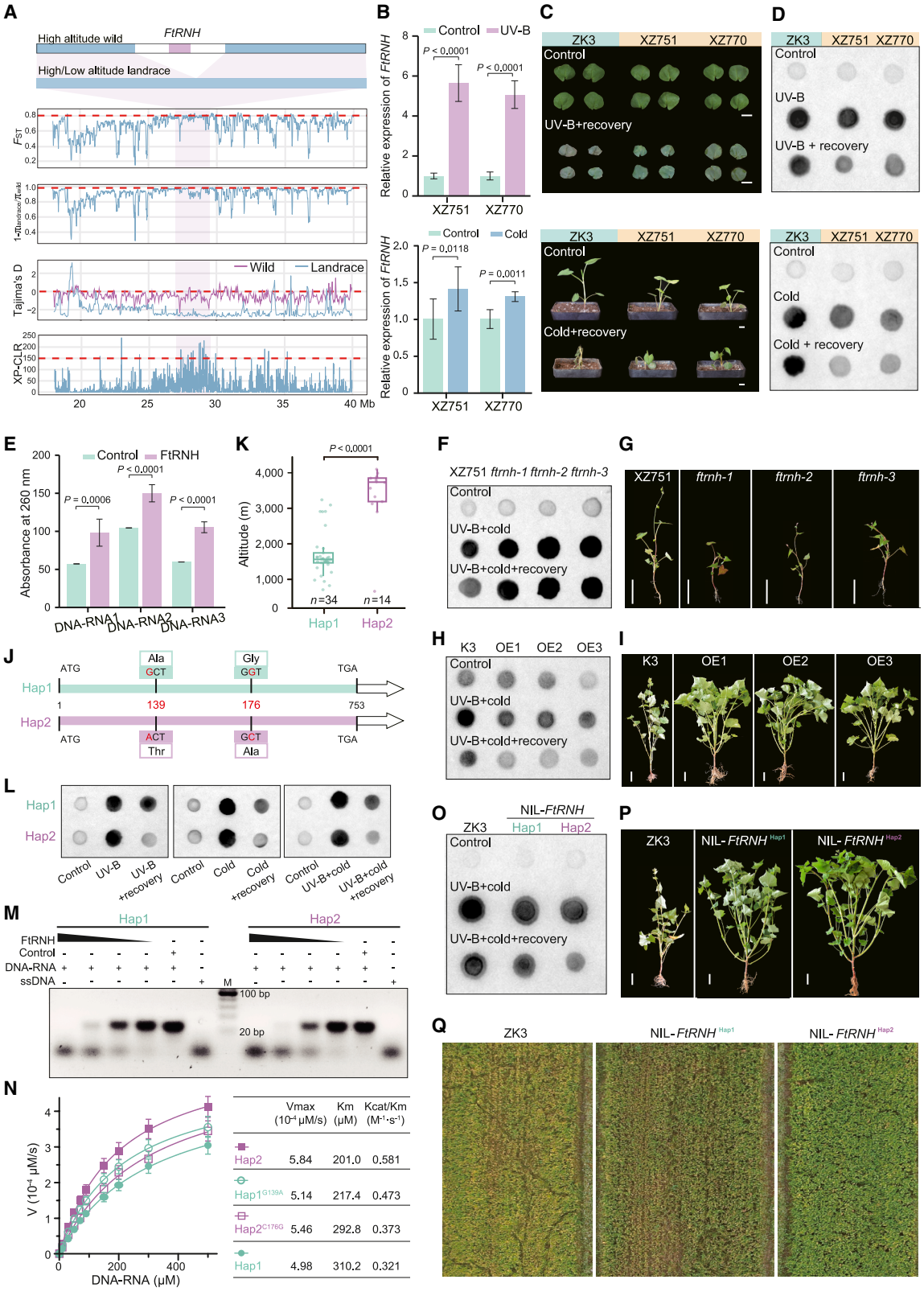

(legend on next page)

Please cite this article in press as: Zhang et al., Pangenome-guided breeding restores high-altitude adaptation and improves yield in Tartary buckwheat, Cell (2026), https://doi.org/10.1016/j.cell.2026.07.035

Table S3B) is situated in an SV hotspot where HW accessions exhibited more SVs than cultivated NL and SL landraces (Figure 2E; Table S2L). Further analysis indicated that *FtRNH* is present in high-altitude HW wild accessions XZ770 and XZ751 (Figure 3A). It has also been reported in another high-altitude wild relative (*F. dibotrys*) in the Himalayan region[24] but is absent in all cultivated landraces, including those grown in the Himalayan and low-altitude regions.

Population genomic analyses revealed higher divergence (1%) in the *FtRNH* region compared with other genomic regions (Figure 3A). Cultivated populations showed a drastic reduction in nucleotide diversity ($\pi = 4.39 \times 10^{-4}$) compared with wild populations ($\pi = 3.81 \times 10^{-3}$), with significantly negative Tajima's D values (approximately -2.0), while wild populations exhibited a neutral pattern (Tajima's D $\approx$ 0). LD analyses suggested that cultivated populations displayed abnormally slow LD decay. At a physical distance of 50 Kb, the linkage strength in cultivated populations ($R^2 \approx 0.79$) was nearly double that in wild populations ($R^2 \approx 0.40$). A fine-scale scan within the high-LD block upstream of *FtRNH* identified an XP-CLR selection peak (score = 61, representing the top 7.93% of genome-wide scores) approximately 50 Kb upstream of the *FtRNH* locus. Consistent with these findings, genetic diversity decreased while genetic divergence increased in this region compared with most other regions of Chr7 (Figure S2O). These patterns suggest a likely hitchhiking scenario, in which artificial selection initially acted on favorably linked variants to improve agronomic traits, resulting in a selective sweep that co-fixed the loss of *FtRNH* due to strong linkage ($R^2 > 0.7$). However, alternative explanations, such as relaxed selection on UV-B and cold tolerance in low-altitude environments, cannot be ruled out.

To explore the potential role of *FtRNH* in high-altitude adaptability, we conducted redundancy analysis correlating its presence with climatic factors (Figure S2P; Table S3C). We observed a correlation with environmental factors, particularly growing-season temperatures (R^2 = 0.08) and intense UV-B radiation (R^2 = 0.08; Figure S2Q), although imbalanced sampling, especially fewer wild accessions from high altitudes, may weaken such correlations, and other factors, including precipitation and soil composition, may also contribute to the specific distribution of *FtRNH* and require further investigation. As a gene specific to wild Tartary buckwheat within the *RNH* family (Figure S2R), *FtRNH* possesses a promoter containing light- and cold-responsive elements, such as G-box, GATA motifs, and MYB- and MYC-binding motifs[25–29] (Figure S2S). We then subjected high-altitude wild accessions (XZ751 and XZ770, with *FtRNH*) and the widely cultivated ZK3 (without *FtRNH*) to UV-B and cold treatments. RT-qPCR demonstrated that *FtRNH* expression was significantly upregulated following UV-B or cold treatment (Figure 3B). The wild accessions showed significantly greater resistance to UV-B and enhanced cold tolerance than ZK3 (Figure 3C). Given that ribonuclease H homologs in other species selectively degrade RNA strands in RNA-DNA hybrids (R-loops) to maintain genome stability,[30–34] we examined R-loop dynamics (Figure 3D; Figure S3A). Following UV-B, cold, or combined treatments, R-loop levels increased significantly in all accessions. However, upon recovery, R-loop levels in wild accessions possessing *FtRNH* were significantly lower than in ZK3, indicating more efficient R-loop clearance. Additionally, levels of cyclobutane pyrimidine dimers (CPDs) and 6–4 photoproducts (6-4PPs), two major UV-B-induced DNA lesions,

Figure 3. The private gene *FtRNH* in wild accession XZ751 contributes to high-altitude adaptability in Tartary buckwheat

(A) From top to bottom: local alignment showing PAV-derived private genes in Himalayan wild Tartary buckwheat genomes. Chromosomal feature distribution of selection signatures on chromosome 7, including F_{ST} between wild and cultivated populations (the red dashed line indicates the top 1% threshold of chromosome-wide distribution), 1 - $\pi_{landrace}/\pi_{wild}$ (high values indicate severe loss of nucleotide diversity in landraces relative to wild populations), Tajima's D of landraces and wild populations, and XP-CLR (landraces vs. wild, ZK3-T2T as reference genome, the red dashed line indicates the top 1% threshold of chromosome-wide distribution). Pink shaded band represents the candidate selective sweep interval harboring *FtRNH*.

(B) *FtRNH* expression before and after UV-B or cold treatment. Data are shown as mean with 95% CIs. *p* values were calculated using two-way ANOVA. *n* = 3.

(C) UV-B and cold resistance phenotypes of Tartary buckwheat varieties ZK3, XZ751, and XZ770. Bar, 1 cm.

(D) Dot plot assay exhibiting R-loop accumulation in ZK3, XZ751, and XZ770 under UV-B or cold treatment and 2-day recovery.

(E) Quantification of the efficiency of FtRNH-His protein hydrolysis of three DNA-RNA hybrid substrates (DNA-RNA1/2/3) by 260 nm absorbance assay, with empty His-tag protein as control, and increased absorbance represents DNA-RNA hybrid degradation into single-stranded nucleic acids. Data are shown as mean with 95% CIs. *p* values were calculated using two-way ANOVA. *n* = 3.

(F) Dot plot assay exhibiting R-loop accumulation in XZ751 and its *ftrnh* mutants under combined UV-B and cold treatment or after 2-day recovery.

(G) Phenotype of wild accession XZ751 and *ftrnh* mutants grown at high altitude (3,500 m).

(H) Dot plot assay exhibiting the R-loop accumulation in K3 and *FtRNH*-overexpressing Tartary buckwheat lines under combined UV-B and cold treatment or after 2-day recovery.

(I) Phenotypes of K3 and *FtRNH*-overexpressing Tartary buckwheat lines grown at high altitude (3,500 m).

(J) Schematic representation of genomic sequence differences between the two *FtRNH* haplotypes (Hap1 and Hap2) in wild Tartary buckwheat accessions.

(K) Altitudinal distribution of wild Tartary buckwheat accessions carrying *FtRNH*-Hap1 vs. *FtRNH*-Hap2. *p* value was calculated using Student's *t* test.

(L) Dot plot assay showing R-loop accumulation in wild Tartary buckwheat harboring *FtRNH*-Hap1 or *FtRNH*-Hap2 under single, combined UV-B and cold stress, as well as 2-day post-stress recovery.

(M) Agarose gel electrophoresis analysis of ribonuclease H activity between two haplotypes. Black wedge indicates decreasing FtRNH concentrations (5, 1, 0.5, and 0.25 μM). DNA-RNA, DNA-RNA hybrid substrate. ssDNA, single-stranded DNA. Control, His-tagged protein (empty vector).

(N) Enzyme kinetic analysis of Hap1, Hap2, and mutants $Hap1^{G139A}$ and $Hap2^{C176G}$ using fluorescently labeled DNA-RNA hybrid strands as substrates. Km, the Michaelis constant. $V_{max.}$, maximum reaction rate. $K_{cat.}$/Km, catalytic efficiency. Data are presented as means ± SD; *n* = 3 independent experiments.

(O) Dot plot assay showing R-loop accumulation in ZK3, NIL-$FtRNH^{Hap1}$, and NIL-$FtRNH^{Hap2}$ under combined UV-B and cold stress, as well as 2-day post-stress recovery.

(P) Phenotypes of ZK3, NIL-$FtRNH^{Hap1}$, and NIL-$FtRNH^{Hap2}$ grown at high altitude (3,500 m).

(Q) Field phenotypes of ZK3, NIL-$FtRNH^{Hap1}$, and NIL-$FtRNH^{Hap2}$ under high-altitude field cultivation (3,500 m).

In (D), (F), (H), (L), and (O), signal intensity represents relative R-loop content. In (G), (I) and (P), bar = 5 cm.

Please cite this article in press as: Zhang et al., Pangenome-guided breeding restores high-altitude adaptation and improves yield in Tartary buckwheat, Cell (2026), https://doi.org/10.1016/j.cell.2026.07.035

increased in all accessions following UV-B treatment but were resolved more efficiently in wild accessions upon recovery (Figures S3B and S3C). Although cold stress alone did not induce these lesions, combined UV-B and cold treatment markedly increased them, with wild accessions again showing significantly lower CPDs and 6-4PPs levels. Comet assays revealed that wild accessions displayed less DNA strand breakage than ZK3 after UV-B, cold, or combined stress, suggesting greater genomic stability (Figure S3D). Consequently, early DNA damage response (γ-H2AX focus formation) and cell death (TUNEL positivity) were significantly reduced in wild accessions following individual or combined stress, compared with ZK3 (Figure S3E). These analyses suggest that *FtRNH* may enhance high-altitude adaptability through R-loop regulation and DNA damage repair.

Functional verification of *FtRNH* in UV-B and cold stress tolerance

To investigate the functional role of *FtRNH* in UV-B and cold stress tolerance, we first assessed whether the protein can degrade RNA within DNA-RNA hybrids *in vitro*. Incubation of hybrid substrates with purified FtRNH-His protein showed that, with increasing FtRNH-His concentrations, the band intensity of all substrates decreased in a concentration-dependent manner, while the corresponding single-stranded DNA product bands increased (Figure S3F), demonstrating that FtRNH-His specifically cleaves the RNA component of DNA-RNA hybrids. Absorbance measurements further confirmed this activity, with all hybrid substrates exhibiting increased absorbance at 260 nm upon FtRNH-His addition compared with controls (Figure 3E). This increase in absorbance reflects the exposure of more nucleotide bases (which absorb strongly at 260 nm) as double-stranded DNA-RNA hybrids are degraded into single-stranded nucleic acids. Subcellular localization analysis revealed that FtRNH localizes to both the cytoplasm and nucleus (Figure S3G), suggesting its potential to recognize and resolve R-loop structures within the nucleus.

To verify its function *in vivo*, we generated *FtRNH* ethyl methanesulfonate (EMS) mutants in the wild accession XZ751. Following UV-B or cold stress, mutants showed more severe damage than the wild type (Figure S3H) and retained significantly higher levels of R-loops after UV-B, cold, or combined stress followed by recovery (Figure 3F; Figure S3A). This impairment in R-loop resolution correlated with exacerbated DNA damage, as evidenced by greater accumulation of UV-B-induced lesions (CPDs and 6-4PPs; Figures S3B and S3C), increased DNA strand breaks (comet assay; Figure S3D), stronger activation of the DNA damage response (γ-H2AX foci), and elevated cell death (TUNEL assay; Figure S3E). We further evaluated the performance of mutants in a native high-altitude environment, where they displayed poorer growth than XZ751 (Figure 3G; Table S3D). Conversely, *FtRNH*-overexpressing lines (Figure S3I) exhibited significantly enhanced resistance to UV-B and cold stress (Figure S3H), associated with more efficient R-loop clearance (Figure 3H; Figure S3A) and reduced DNA damage markers, including CPDs/6-4PPs lesions (Figures S3B and S3C), DNA strand breaks (Figure S3D), γ-H2AX foci, and TUNEL signals (Figure S3E). Under high-altitude conditions, overexpression lines grew significantly better than the control (Figure 3I; Table S3D).

Compared with controls, both *FtRNH* mutant and overexpression caused widespread transcriptome changes (Table S3E). Among these, the expression of genes involved in flavonoid biosynthesis and antioxidant pathways was decreased in mutants and increased in overexpression lines (Figure S4A). Correspondingly, after UV-B, cold, or combined stress, flavonoid accumulation and antioxidant enzyme activities were significantly lower in mutants and higher in overexpression lines (Figure S4B). Since flavonoids and antioxidant enzymes contribute to UV-B and cold stress resistance,[9–11,35] these pathways likely participate in *FtRNH*-involved high-altitude adaptation. To determine whether *FtRNH* influences these pathways via R-loop resolution, we performed DNA:RNA immunoprecipitation followed by sequencing (DRIP-seq) under stress conditions (Figure S4C; Table S3F). Overexpression of *FtRNH* led to decreased R-loop accumulation across many genomic loci, including, but not limited to, genes involved in flavonoid biosynthesis and the antioxidant systems, while *FtRNH* mutants resulted in increased R-loop accumulation at these loci (Figure S4C), suggesting broader functions beyond these specific pathways. To test whether FtRNH can directly act on R-loops on these genes, we synthesized R-loop substrates corresponding to key pathway genes and demonstrated that purified FtRNH-His effectively degrades them *in vitro* (Figure S4D), indicating that FtRNH can resolve R-loops at these loci. Furthermore, treatment of *FtRNH*-overexpressing plants with the flavonoid biosynthesis inhibitor 2-aminoindan-2-phosphonic acid (AIP) significantly attenuated, though did not completely abolish, the stress resistance advantage (Figure S4E). Additionally, exogenous application of flavonoids or H_2O_2 upregulated *FtRNH* expression (Figure S4F). These findings suggest that *FtRNH* coordinates an adaptive feedback loop for high-altitude stress resilience: UV-B and cold stress induce *FtRNH* expression, and accumulated flavonoids further feedback to promote it, thereby continuously amplifying genome protection and defense metabolism (Figure S4G). Finally, to examine whether wild Tartary buckwheat-specific *FtRNH* could confer tolerance in other species, we expressed it in the eudicot *Arabidopsis thaliana* and the monocot rice. In both species, *FtRNH*-overexpressing lines exhibited visibly greater resistance to UV-B, cold, or combined stress than wild-type plants (Figures S4H and S4I). Together, these results demonstrate that *FtRNH* enhances tolerance to high-altitude stresses not only in buckwheat but also in heterologous plant systems.

Allelic variation and the superior allele of *FtRNH* across wild accessions

To analyze the natural variation in *FtRNH*, we used resequencing data from 994 accessions aligned to the *FtRNH* sequence of wild accession XZ751. Only 48 Himalayan wild accessions exhibited high coverage depth in the *FtRNH* region, while all cultivated landraces showed zero coverage (Figure S4J). Sequence analysis of *FtRNH* in these 48 wild accessions revealed two haplotypes, defined by missense mutations at Ala47Thr and Gly59Ala within the functional domain of FtRNH (Figure 3J). Notably, accessions carrying Hap2 were generally found at higher altitudes than those carrying Hap1 (which includes XZ751 and XZ770; Figure 3K), suggesting a potential adaptive

Please cite this article in press as: Zhang et al., Pangenome-guided breeding restores high-altitude adaptation and improves yield in Tartary buckwheat, Cell (2026), https://doi.org/10.1016/j.cell.2026.07.035

CellPress

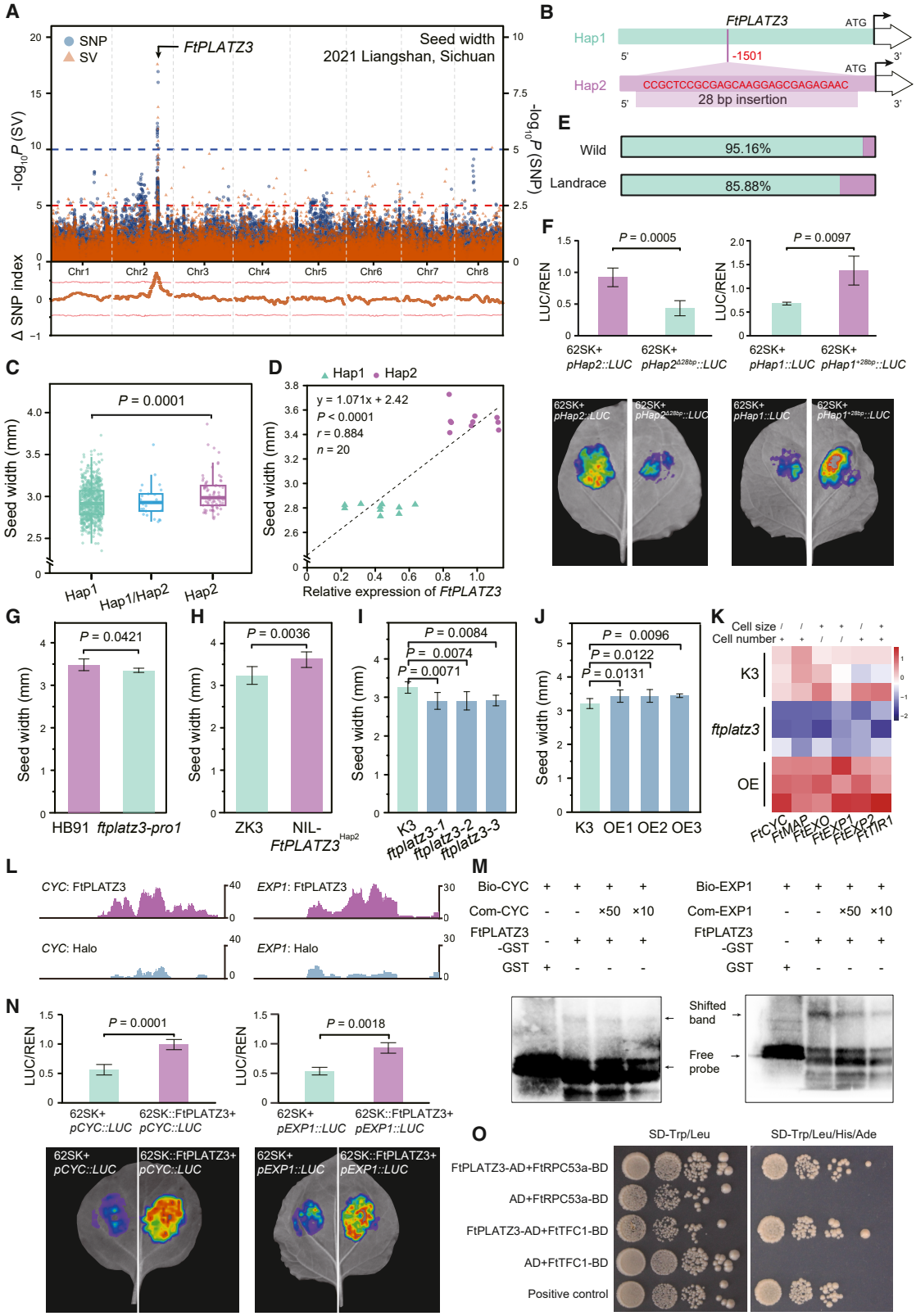

(legend on next page)

Please cite this article in press as: Zhang et al., Pangenome-guided breeding restores high-altitude adaptation and improves yield in Tartary buckwheat, Cell (2026), https://doi.org/10.1016/j.cell.2026.07.035

advantage of Hap2 in more extreme environments. Consistent with this ecological distribution, accessions carrying Hap2 cleared stress-induced R-loops more efficiently than Hap1 after UV-B, cold, or combined stress (Figure 3L). They also accumulated lower levels of DNA damage markers, including CPDs/6-4PPs lesions (Figures S4K and S4L), DNA strand breaks (Figure S4M), γ-H2AX foci, and TUNEL signals (Figure S4N). Hap2 also exhibited higher ribonuclease H activity, producing more single-stranded DNA product than Hap1 (Figure 3M), with higher maximum reaction velocity ($V_{max.}$) and a lower Michaelis constant (Km) (Figure 3N). Consequently, the catalytic efficiency ($K_{cat.}$/Km) of Hap2 was significantly greater than that of Hap1. Site-directed mutagenesis of the two specific amino acid residues in Hap2 partially reduced $V_{max.}$, increased Km, and decreased $K_{cat.}$/Km, confirming their direct contribution to the superior activity of the Hap2 variant.

To further validate the functional superiority of Hap2 *in planta*, we developed two near-isogenic lines (NILs) in the ZK3 background: NIL-*FtRNH*^{Hap1} (containing *FtRNH*-Hap1 from XZ751) and NIL-*FtRNH*^{Hap2} (containing *FtRNH*-Hap2 from XZ625). Under normal conditions, both NILs were phenotypically similar to ZK3 (Table S3D). However, after UV-B, cold, or combined stress, both NILs exhibited stronger growth than ZK3, with NIL-*FtRNH*^{Hap2} outperforming NIL-*FtRNH*^{Hap1} (Figure S4O). Mechanistically, the NILs, particularly NIL-*FtRNH*^{Hap2}, showed more efficient clearance of R-loops (Figure 3O; Figure S4P) and reduced accumulation of DNA damage markers (Figures S4K–S4N) compared with ZK3 after stress recovery. Field trials under natural high-altitude conditions further demonstrated that both NILs grew better than ZK3, with NIL-*FtRNH*^{Hap2} again showing the best performance (Figures 3P and 3Q; Figure S4O). These results indicate that the Hap2 variant of *FtRNH* possesses a greater capacity to resolve R-loops and mitigate subsequent DNA damage, aligning with its survival advantage at higher altitudes.

Pangenome-based GWAS identification of the SV associated with seed-size variation

Seed size is a key agronomic trait influencing crop yield. Using a graph-based pangenome and phenotypic data on seed width and length collected from common garden experiments, we performed GWAS on 994 accessions, integrating both SVs (≥20 bp) and SNPs. A total of 14 loci encompassing 623 genes were identified through SV-GWAS and SNP-GWAS (Table S4A). Among these, 65 genes were repeatedly associated with the same trait across at least two independent measurements or in common garden experiments at two distinct locations (Table S4A). A significant locus on chromosome 2 was consistently associated with seed width (Figure 4A; Figure S5A) and corresponded to *qClu1-5*, a quantitative trait locus (QTL) cluster previously reported to be repeatedly linked to grain length, width, and length-to-width ratio in a Tartary buckwheat recombinant inbred line (RIL) population across four different environments[36] (Figure 4A; Table S4B), indicating this region is a key determinant of seed size. Further dissection of this locus revealed tandem duplications of genes encoding plant AT-rich sequence and zinc-binding transcription factors (PLATZ) (Figures S5B and S5C). RT-qPCR showed that these genes were highly expressed during the GS1 stage (grain stage 1, seed formation initiation) compared with GS2 (filling) and GS3 (milk-ripe) stages in ZK3, with *FtPLATZ3* (*ZK3006110*) showing the highest expression (Figure S5B), suggesting its potential role in seed-size regulation.

We next examined sequence variations in *FtPLATZ3* and found that a 28-bp insertion in its promoter was significantly associated with seed width, whereas other non-rare mutations in the vicinity showed no such association (Figures 4B and 4C; Tables S4B and S4C). Landraces carrying Hap2 (with the insertion) produced wider seeds and displayed higher *FtPLATZ3* expression than landraces carrying Hap1 (without the insertion) (Figures 4C and 4D). Both haplotypes were also present in Himalayan wild accessions (Figure 4E). Deletion of the 28-bp sequence in the Hap2 background significantly reduced promoter activity, while its insertion into the Hap1 background enhanced promoter activity, confirming that this 28-bp element is a functional *cis*-regulatory variant (Figure 4F). This sequence contains several putative transcription-binding motifs, and mutation of these motifs reduced promoter activity (Figure S5D). To validate its functional impact, we knocked out this insertion in an accession carrying Hap2 (HB91). Knockout lines exhibited

Figure 4. Identification of *FtPLATZ3* and its CNV associated with seed size in Tartary buckwheat

(A) Upper: Manhattan plots from SV- and SNP-based GWAS for seed width (dashed line indicates significance threshold [$-\log_{10}p = 5$]). Lower: genomic region associated with seed size identified by QTL mapping.

(B) Schematic representation of genomic sequence differences between the two *FtPLATZ3* haplotypes.

(C) Boxplots showing seed width in accessions carrying the two haplotypes. *p* value was calculated using one-way ANOVA.

(D) *FtPLATZ3* expression levels in accessions carrying the two haplotypes. $n = 10$ per haplotype.

(E) Frequency distribution of the two *FtPLATZ3* haplotypes in wild Tartary buckwheat versus cultivated landraces.

(F) The 28-bp insertion is a positive *cis*-element for *FtPLATZ3* promoter activity, as shown by luminescence intensity in *Nicotiana benthamiana*. Compared with the wild-type Hap2 promoter, the 28-bp deleted version (*pHap2*$^{\Delta 28bp}$) showed drastically decreased activity, whereas inserting the fragment into Hap1 (*pHap1*$^{+28bp}$) significantly elevated it. Data are presented as mean with 95% CIs. *p* values were calculated using Student's *t* test. $n = 3$

(G–J) Seed width of (G) HB91 and *ftplatz3-pro1*, (H) ZK3 and NIL-*FtPLATZ3*^{Hap2}, (I) K3 and its *FtPLATZ3* mutants, (J) K3 and *FtPLATZ3*-overexpressing (OE) lines. $n = 3$. Data are presented as mean with 95% CIs. *p* values were calculated using (G) and (H) Student's *t* test and (I and J) one-way ANOVA.

(K) Differentially expressed genes involved in cell division in the transcriptome of *FtPLATZ3*-overexpression or mutants.

(L) DAP-seq binding peaks of FtPLATZ3 at the loci of downstream target genes *FtCYC* and *FtEXP1*. Empty Halo-tagged protein served as the negative control.

(M) EMSA validation of direct binding between FtPLATZ3 and the promoters of *FtCYC* and *FtEXP1*.

(N) FtPLATZ3 acts as a transcriptional activator to promote the promoter activity of downstream target genes *FtCYC* and *FtEXP1*. The promoters of *FtCYC* and *FtEXP1* were used as reporters and were co-infiltrated with an empty 62SK or 62SK-*FtPLATZ3* effector in *N. benthamiana* leaves. Data are presented as mean with 95% CIs. *p* values were calculated using Student's *t* test. $n = 3$.

(O) Yeast two-hybrid assay showing interactions between FtPLATZ3 and FtRPC53a/FtTFC1. Transformed yeast cells were grown on SD (-Leu/Trp) and SD (-Leu/Trp/His/Ade) media to assess protein-protein interactions.

Please cite this article in press as: Zhang et al., Pangenome-guided breeding restores high-altitude adaptation and improves yield in Tartary buckwheat, Cell (2026), https://doi.org/10.1016/j.cell.2026.07.035

significantly reduced seed size (Figure 4G). Conversely, an NIL (NIL-*FtPLATZ3*^{Hap2}) carrying *FtPLATZ3*-Hap2 from HB91 in the ZK3 (Hap1) background showed increased seed width (Figure 4H). Together, these results demonstrate that the 28-bp promoter SV in *FtPLATZ3* plays a critical role in modulating seed-size variation in Tartary buckwheat.

Further functional characterization of *PLATZ3* in seed-size regulation across plant species

To further investigate *FtPLATZ3* function, we examined its tissue-specific expression at the full-bloom stage and spatial distribution within seeds at the GS1 stage. *FtPLATZ3* was predominantly expressed in the embryonic region (Figure S5E). Subcellular localization assays revealed that FtPLATZ3 localizes to the nucleus (Figure S5F), consistent with its putative role as a transcription factor. To assess its *in vivo* function, we generated *FtPLATZ3* knockout lines in the K3 background. These mutants exhibited significantly reduced seed width (Figure 4I), accompanied by decreased endosperm cell number and size (Figures S5G and S5H). Conversely, *FtPLATZ3* overexpression lines (Figure S5I) showed increased seed width (Figure 4J) and increased endosperm cell number and size (Figures S5J and S5K). Transcriptome analyses revealed that genes encoding cell cycle-related proteins (e.g., cyclins, CYC) and cell expansion factors were significantly upregulated in overexpression lines and downregulated in knockout lines (Figure 4K; Table S4D). DNA affinity purification sequencing (DAP-seq), electrophoretic mobility shift assays (EMSA), and dual-luciferase reporter assays demonstrated that FtPLATZ3 directly regulates these genes (Figures 4L–4N; Table S4E).

Previous studies showed that the rice ortholog of *FtPLATZ3* (Os06g0666100) positively regulates seed development through interaction with RNA polymerase III (RNAPIII) subunit C53 (RPC53) and transcription factor class C1 (TFC1), both essential components of the RNAPIII transcription complex.[37–39] To test whether *FtPLATZ3* acts through a conserved mechanism, we performed yeast two-hybrid assays using Tartary buckwheat orthologs *FtTFC1* and *FtRPC53a*. Both FtRPC53a and FtTFC1 interacted with FtPLATZ3 (Figure 4O; Figure S5L), suggesting that *FtPLATZ3* may act via an RNAPIII-mediated pathway. Furthermore, transgenic *Arabidopsis thaliana* lines overexpressing *FtPLATZ3* exhibited increased seed width (Figure S5M), and heterologous expression of *FtPLATZ3* in rice also produced longer seeds (Figure S5N). Collectively, these results demonstrate that PLATZ3 functions as a conserved transcription factor regulating seed development across plant species.

We next investigated whether CNV of tandemly duplicated *FtPLATZ* genes (Figure S5B) affects seed width. Himalayan wild buckwheat and high-altitude landraces harbor fewer *FtPLATZ* copies than low-altitude landraces (Figure S5O). Although *FtPLATZ3* and its orthologs showed the highest expression during the GS1 stage, other tandem copies were also transcriptionally active (Figure S5P). Knocking out one or the two proximal copies reduced seed width (Figure S5Q), with double-mutants showing a stronger effect, indicating that CNV at this locus contributes to seed-size differences between high- and low-altitude accessions. Expression of these tandem genes was not altered by UV-B or cold stress (Figure S5R), suggesting their seed-growth-promoting function is constitutively maintained. Thus, they represent robust targets for yield improvement even in stress-prone high-altitude regions.

Breeding an ideal Tartary buckwheat cultivar with high-altitude adaptability and enhanced field yield

To accelerate breeding of Tartary buckwheat for the high-altitude Himalayan region, we integrated favorable SV alleles (including CNVs) from both high-altitude wild accessions and low-altitude landraces. We first evaluated NIL-*FtRNH*^{Hap2}, created by introgressing the *FtRNH*-Hap2 allele from wild accession XZ625 into ZK3 (which carries the 28-bp deletion allele *FtPLATZ3*-Hap1). Although NIL-*FtRNH*^{Hap2} exhibited similar seed size and weight to ZK3 (Figures 5A and 5B), it showed superior growth and biomass at high altitude, resulting in significantly higher field yield (Figure 5C), attributed to enhanced high-altitude fitness from *FtRNH*-Hap2.

To further increase yield potential, we introduced both *FtPLATZ3*-Hap2 (carrying the large-seed-associated 28-bp insertion) and additional *FtPLATZ* copies. We crossed NIL-*FtRNH*^{Hap2} with NIL-*FtPLATZ3*^{Hap2} and self-pollinated the progeny to obtain homozygous lines harboring both *FtRNH*-Hap2 and *FtPLATZ3*-Hap2, designated NIL-*FtRNH*^{Hap2}-*FtPLATZ3*^{Hap2}. Subsequently, we identified an unequal recombination in the selfed progeny derived from a cross between this line and the wild accession XZ625 (Figure S5O). Through backcrossing to the NIL-*FtRNH*^{Hap2}-*FtPLATZ3*^{Hap2} parent and marker-assisted selection, we successfully generated a progeny line named NIL-*FtRNH*^{Hap2}-*FtPLATZ3*^{Hap2}-MC (more copy). This line produced significantly larger seeds than NIL-*FtRNH*^{Hap2} even at low altitude (Figures 5A and 5B). Importantly, at high altitudes, it retained adaptive advantages, exhibiting higher biomass than ZK3 and higher field yield than both ZK3 and the parental NIL-*FtRNH*^{Hap2} (Figure 5C; Table S4F). By combining robust high-altitude performance with enhanced seed size and yield traits, NIL-*FtRNH*^{Hap2}-*FtPLATZ3*^{Hap2}-MC represents a promising candidate buckwheat cultivar for the high-altitude Himalayan region (Figure 5D).

DISCUSSION

Plants have evolved complex adaptive mechanisms to mitigate multiple environmental stresses.[40–45] The Himalayan region presents intense UV-B radiation and cold stress that typically preclude crop cultivation. Yet native wild plants have evolved protective traits. Many beneficial "super alleles" may have been lost during domestication of crops such as Tartary buckwheat, which were historically cultivated in more sheltered, low-altitude valleys of the same region.[46] As documented in other species, such advantageous alleles are often retained in wild relatives inhabiting more extreme, high-altitude niches and can be systematically uncovered through pangenomic analyses.[47–49] Our study discovered that *FtRNH*, involved in mitigating UV-B-induced DNA damage, is specifically retained in wild Tartary buckwheat from the high-altitude Himalayas but absent in landraces, suggesting that *FtRNH* may have been lost during initial domestication, possibly for other linked traits in lower-altitude

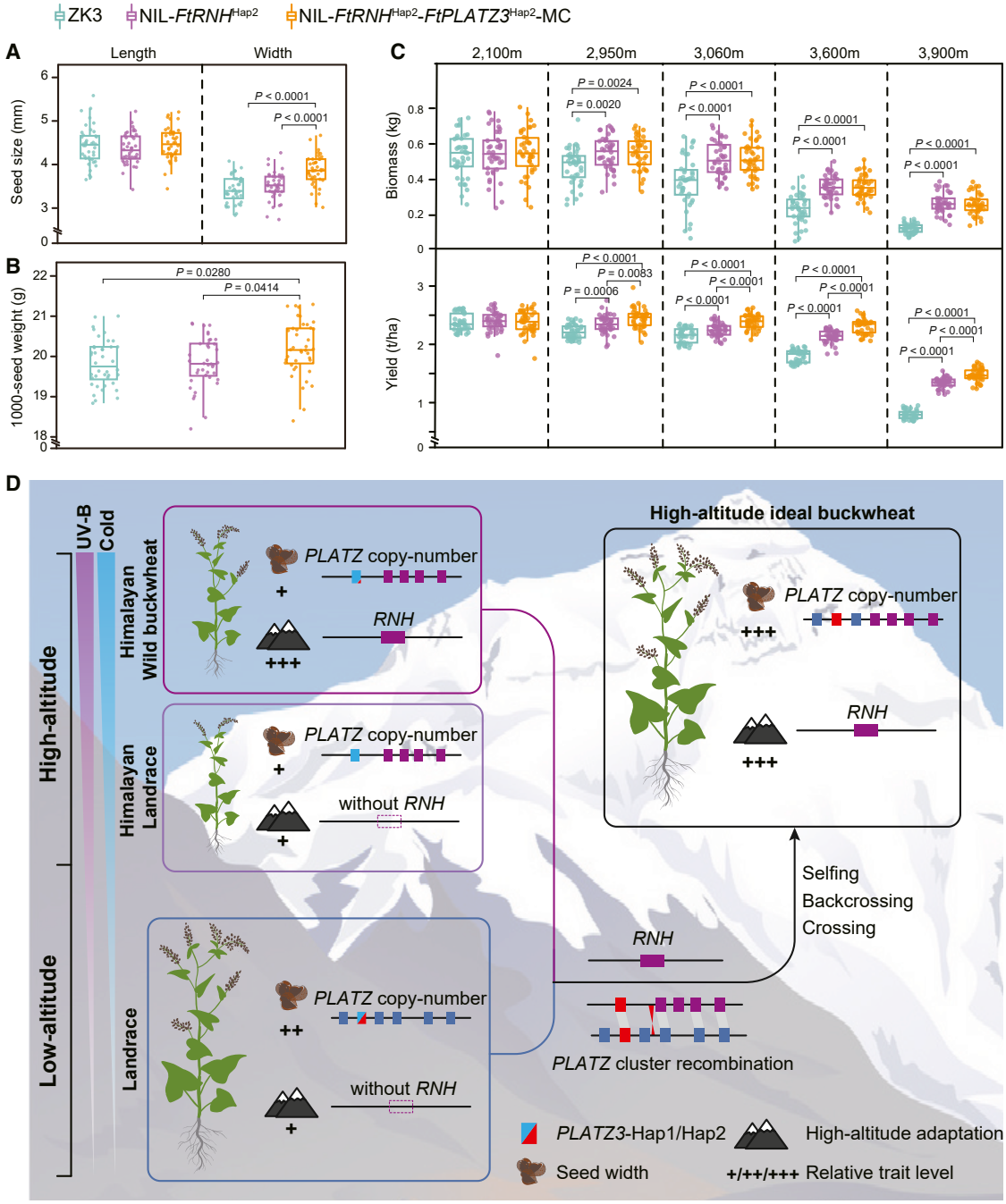

Figure 5. Pangenome assisted the breeding of Tartary buckwheat with improved seed size and high-altitude adaptability

(A–C) Seed size (A), 1,000-seed weight (B), biomass and grain yield at different altitudes (C) of ZK3, NIL-*FtRNH*^{Hap2}, and NIL-*FtRNH*^{Hap2}-*FtPLATZ3*^{Hap2}-MC. Data shown represent one independent field plot. *p* values were calculated using one-way ANOVA (A) and (B) and two-way ANOVA (C). *n* = 40.

(D) Schematic overview of the pangenome-assisted breeding strategy. High-altitude wild accessions carry *FtRNH* (conferring high-altitude adaptability), whereas cultivated landraces (both high- and low-altitude) lack it. High-altitude accessions (wild and cultivated) typically harbor few copies of *FtPLATZ*, with most wild accessions and all high-altitude landraces carrying the small-seed haplotype (*FtPLATZ3*-Hap1). Low-altitude landraces possess more *FtPLATZ* copies, with ~15% carrying the large-seed haplotype (*FtPLATZ3*-Hap2). To develop a high-yielding variety adapted to high-altitude, we introgressed *FtRNH* (from a high-altitude wild accession) and the large-seed *FtPLATZ3*-Hap2 allele into ZK3 (which lacks *FtRNH* and carries *FtPLATZ3*-Hap1). Furthermore, we increased *FtPLATZ* copy number through unequal recombination, generating NIL-*FtRNH*^{Hap2}-*FtPLATZ3*^{Hap2}-MC, which combines high-altitude adaptability with a large-seed phenotype.

environments and/or the alleviated selection pressure from high-altitude stressors.

Concurrently, enhancing seed size remains a major objective for improving crop yield.[50,51] Our pangenomic analyses of both low-altitude landraces and high-altitude wild Tartary buckwheat accessions suggest that seed-size variation is associated with *FtPLATZ* SVs, including CNVs and a promoter insertion in *FtPLATZ3*. Low-altitude landraces with larger seeds were characterized by higher *FtPLATZ* copy number and a 28-bp insertion. This insertion is also present in wild accessions, suggesting that different domestication events or backcrossing with certain wild accessions introduced this SV into some landraces. However, the increased *FtPLATZ* copy number in some landraces may have arisen from artificial crossing or natural variation during long-term breeding practices. Collectively, our pangenome analysis thus pinpointed independent beneficial alleles for highland breeding of Tartary buckwheat: one governing high-altitude adaptability (*FtRNH* from wild accessions) and the other controlling seed size (*FtPLATZ* CNV and 28-bp insertion).

The strategic integration of superior alleles from diverse genetic pools represents a powerful approach for crop improvement.[52,53] We devised a crossing scheme combining the favorable *FtRNH* allele from wild accessions, conferring high-altitude adaptability in Tartary buckwheat, and the superior *FtPLATZ* haplotypes associated with increased seed size, namely the *FtPLATZ3* promoter insertion and elevated *FtPLATZ* copy number. This approach enabled the successful development of a hybrid line exhibiting both enhanced high-altitude adaptability and significantly improved yield. Our findings provide valuable genomic resources for precision breeding in Tartary buckwheat and demonstrate a generalizable strategy for integrating beneficial alleles, including CNVs, from both wild relatives and local landraces to accelerate elite crop improvement.

Limitations of the study

Although we demonstrate that all *FtRNH* is present in high-altitude wild populations of Tartary buckwheat and that the genomic region surrounding its absence in low-altitude landraces has undergone strong artificial selection, the specific gene(s) within this linked region responsible for other favorable domestication traits, and the phenotypes they confer, remain unidentified. Furthermore, the loss of *FtRNH* might also stem from relaxed selection on environmental tolerance at low altitude rather than exclusively through passive hitchhiking. Future studies should systematically dissect this region through targeted gene knockout, allelic replacement, and comprehensive phenotypic characterization to recover these genes and elucidate their underlying mechanisms. Moreover, high-altitude adaptability is a complex polygenic trait. While our findings indicate that the *Fagopyrum*-specific *FtRNH* contributes to this process by promoting R-loop resolution and DNA damage repair in Tartary buckwheat, whether it interacts with other genes during this process remains unknown. Its broader role in other plant species and the extent of mechanistic conservation also warrant further investigation. Furthermore, the genome-wide R-loop changes observed in DRIP-seq suggest a broader role of *FtRNH* in transcriptional maintenance, which requires further investigation. Similarly, although we show that increased *FtPLATZ* copy number is associated with large seed size and high yield in Tartary buckwheat landraces, the temporal, spatial, and selective origins of this copy-number expansion remain unknown. When, where, and how this favorable CNV was selected during breeding history has yet to be determined. Whole-genome resequencing of a broader panel of landraces, particularly ancient or historically preserved accessions, may help clarify the evolutionary trajectory of this locus.

RESOURCE AVAILABILITY

Lead contact

Further information and requests for resources and reagents should be directed to and will be fulfilled by the lead contact, Meiliang Zhou (zhoumeiliang@caas.cn).

Materials availability

Materials generated in this study are available from the lead contact.

Data and code availability

- All data generated in this study have been deposited in the Genome Sequence Archive database of the National Genomics Data Center, China National Center for Bioinformation (https://ngdc.cncb.ac.cn) under BioProject: PRJCA036855.
- This paper does not report original code.
- Any additional information required to reanalyze the data reported in this paper is available from the lead contact upon request.

ACKNOWLEDGMENTS

This research was supported by the National Natural Science Foundation of China (32161143005 and W2512019); the Youth Innovation Program of the Chinese Academy of Agricultural Sciences (Y2026QC01 and Y2022QC02); the Science and Technology Projects of the Xizang Autonomous Region, China (XZ202402ZD0005); the National Science Centre, Poland, research project SHENG (2025/56/Q/NZ9/00076); the Asia Cooperation Fund Project (10212524161009000029); the National Key R&D Program of China (2023YFF1002500 and 2022YFE0140800); the National Natural Science Foundation of China (32301794 and 31501365); the start-up grant of the Food Futures Institute, Murdoch University, Australia; and the project from the Xizang Special Agricultural and Animal Husbandry Resources Research Collaborative Innovation Center under Provincial-Ministerial Co-construction-Crop Direction Research (XZTSZY202001).

AUTHOR CONTRIBUTIONS

M.Z., X.L., J.L., and R.K.V. conceived and designed the research. M.Z., K.Z., Y.H., and X.L. headed, managed, and coordinated the project. H.L., Y.H., K.Z., M.D., Y.S., A.C., and R.R.M. contributed to genome assembly, pangenomics, and graph-based pangenome analysis. J.H., Z.W., Y.C., W.L., J.L., X.H., M.D., P.Y., Z.C., M.H., A.P., and A.B. contributed to the molecular experiments and construction of transgenic materials. W.L., M.D., and J.L. contributed to the construction and phenotype evaluation of NIL populations. S.-H.W., D.J., M.Q., M.Z., J.G., B.F., Z.Z., D.L., W.L., X.F., D.P.G., N.D., and I.K. participated in the material preparation. Z.C. assisted in bioinformatics analyses. Y.H., K.Z., H.L., J.L., and M.Z. wrote the manuscript. Y.H., H.L., J.L., M.Z., A.R.F., M.S., and R.K.V. revised the manuscript. M.Z. supervised the research. All authors read, edited, and approved the manuscript.

DECLARATION OF INTERESTS

The Institute of Crop Sciences, Chinese Academy of Agricultural Sciences, has one pending patent application based on this study.

STAR★METHODS

Detailed methods are provided in the online version of this paper and include the following:

- KEY RESOURCES TABLE
- EXPERIMENTAL MODEL AND STUDY PARTICIPANT DETAILS
  - Tartary buckwheat (*Fagopyrum tataricum*)
  - Other experimental models
- METHOD DETAILS
  - DNA extraction
  - Genome sequencing, assembly, and quality assessment
  - Genome annotation
  - Genomic collinearity
  - ChIP-seq analysis
  - Cytological analysis
  - Genome resequenced
  - Population genetic analysis
  - Pangenome construction
  - SV identification and graph-based pangenome construction
  - SV genomic feature annotation
  - Pan-graph SV validation
  - Selective sweep identification
  - Phylogenetic analysis of genes
  - Genome-wide association study (GWAS)
  - Transgenic materials construction
  - Development of NILs
  - Plant stress treatments and phenotypic assays
  - Quantitative RT-PCR and RNA-seq
  - Dual-luciferase reporter assay
  - Enzyme activity analysis
  - R-loop level assay
  - DRIP-seq
  - CPDs and 6-4PPs content measurement
  - Comet assay
  - γ-H2AX immunofluorescence assay
  - TUNEL staining
  - Subcellular localization identification
  - Paraffin sectioning
  - EMSA
  - DAP-seq
  - Yeast two-hybrid assay
  - Field planting and yield measurement
- QUANTIFICATION AND STATISTICAL ANALYSIS

SUPPLEMENTAL INFORMATION

Supplemental information can be found online at https://doi.org/10.1016/j.cell.2026.07.035.

Received: September 14, 2025
Revised: February 20, 2026
Accepted: July 23, 2026

REFERENCES

1. International Centre; Integrated; Mountain; Development (2019). The Hindu Kush Himalaya Assessment: Mountains, Climate Change, Sustainability and People (Cham (Switzerland): Springer). https://doi.org/10.1007/978-3-319-92288-1.
2. He, Y., Zhang, K., Shi, Y., Lin, H., Huang, X., Lu, X., Wang, Z., Li, W., Feng, X., Shi, T., et al. (2024). Genomic insight into the origin, domestication, dispersal, diversification and human selection of Tartary buckwheat. Genome Biol. *25*, 61. https://doi.org/10.1186/s13059-024-03203-z.
3. Zhang, K., He, M., Fan, Y., Zhao, H., Gao, B., Yang, K., Li, F., Tang, Y., Gao, Q., Lin, T., et al. (2021). Resequencing of global Tartary buckwheat accessions reveals multiple domestication events and key loci associated with agronomic traits. Genome Biol. *22*, 23. https://doi.org/10.1186/s13059-020-02217-7.
4. Kumari, A., and Chaudhary, H.K. (2020). Nutraceutical crop buckwheat: a concealed wealth in the lap of Himalayas. Crit. Rev. Biotechnol. *40*, 539–554. https://doi.org/10.1080/07388551.2020.1747387.
5. Zeng, X., Guo, Y., Xu, Q., Mascher, M., Guo, G., Li, S., Mao, L., Liu, Q., Xia, Z., Zhou, J., et al. (2018). Origin and evolution of qingke barley in Tibet. Nat. Commun. *9*, 5433. https://doi.org/10.1038/s41467-018-07920-5.
6. Jha, R., Zhang, K., He, Y., Mendler-Drienyovszki, N., Magyar-Tábori, K., Quinet, M., Germ, M., Kreft, I., Meglič, V., Ikeda, K., et al. (2024). Global nutritional challenges and opportunities: Buckwheat, a potential bridge between nutrient deficiency and food security. Trends Food Sci. Technol. *145*, 104365. https://doi.org/10.1016/j.tifs.2024.104365.
7. Joshi, D.C., Zhang, K., Wang, C., Chandora, R., Khurshid, M., Li, J., He, M., Georgiev, M.I., and Zhou, M. (2020). Strategic enhancement of genetic gain for nutraceutical development in buckwheat: A genomics-driven perspective. Biotechnol. Adv. *39*, 107479. https://doi.org/10.1016/j.biotechadv.2019.107479.
8. Huda, M.N., Lu, S., Jahan, T., Ding, M., Jha, R., Zhang, K., Zhang, W., Georgiev, M.I., Park, S.U., and Zhou, M. (2021). Treasure from garden: Bioactive compounds of buckwheat. Food Chem. *335*, 127653. https://doi.org/10.1016/j.foodchem.2020.127653.
9. Bao, H., Yuan, L., Luo, Y., Zhang, J., Liu, X., Wu, Q., Wang, X., Liu, J., and Zhu, G. (2025). The transcription factor WRKY41-FLAVONOID 3′-HYDROXYLASE module fine-tunes flavonoid metabolism and cold tolerance in potato. Plant Physiol. *197*, kiaf070. https://doi.org/10.1093/plphys/kiaf070.
10. Bulut, M., Tohge, T., Chen, W., Luo, J., Wang, Z., Huang, X., Zhou, M., and Fernie, A.R. (2025). Learning from nature: phytochemical strategies to protect against UV-B damage. Nat. Commun. *16*, 9927. https://doi.org/10.1038/s41467-025-66135-7.
11. He, J., Yao, L., Pecoraro, L., Liu, C., Wang, J., Huang, L., and Gao, W. (2023). Cold stress regulates accumulation of flavonoids and terpenoids in plants by phytohormone, transcription process, functional enzyme, and epigenetics. Crit. Rev. Biotechnol. *43*, 680–697. https://doi.org/10.1080/07388551.2022.2053056.
12. Hunt, H.V., Shang, X., and Jones, M.K. (2018). Buckwheat: a crop from outside the major Chinese domestication centres? A review of the archaeobotanical, palynological and genetic evidence. Veg. Hist. Archaeobot. *27*, 493–506. https://doi.org/10.1007/s00334-017-0649-4.
13. Zhao, H., He, Y., Zhang, K., Li, S., Chen, Y., He, M., He, F., Gao, B., Yang, D., Fan, Y., et al. (2023). Rewiring of the seed metabolome during Tartary buckwheat domestication. Plant Biotechnol. J. *21*, 150–164. https://doi.org/10.1111/pbi.13932.
14. Lin, H., Yao, Y., Sun, P., Feng, L., Wang, S., Ren, Y., Yu, X., Xi, Z., and Liu, J. (2023). Haplotype-resolved genomes of two buckwheat crops provide insights into their contrasted rutin concentrations and reproductive systems. BMC Biol. *21*, 87. https://doi.org/10.1186/s12915-023-01587-1.
15. Lai, D., Zhang, K., He, Y., Fan, Y., Li, W., Shi, Y., Gao, Y., Huang, X., He, J., Zhao, H., et al. (2024). Multi-omics identification of a key glycosyl hydrolase gene *FtGH1* involved in rutin hydrolysis in Tartary buckwheat (*Fagopyrum tataricum*). Plant Biotechnol. J. *22*, 1206–1223. https://doi.org/10.1111/pbi.14259.
16. He, Y., Zhang, K., Li, S., Lu, X., Zhao, H., Guan, C., Huang, X., Shi, Y., Kang, Z., Fan, Y., et al. (2023). Multiomics analysis reveals the molecular mechanisms underlying virulence in *Rhizoctonia* and jasmonic acid-mediated resistance in Tartary buckwheat (*Fagopyrum tataricum*). Plant Cell *35*, 2773–2798. https://doi.org/10.1093/plcell/koad118.

17. Du, H., and Liang, C. (2019). Assembly of chromosome-scale contigs by efficiently resolving repetitive sequences with long reads. Nat. Commun. *10*, 5360. https://doi.org/10.1038/s41467-019-13355-3.

18. Kang, M., Wu, H., Liu, H., Liu, W., Zhu, M., Han, Y., Liu, W., Chen, C., Song, Y., Tan, L., et al. (2023). The pan-genome and local adaptation of *Arabidopsis thaliana*. Nat. Commun. *14*, 6259. https://doi.org/10.1038/s41467-023-42029-4.

19. Yan, H., Sun, M., Zhang, Z., Jin, Y., Zhang, A., Lin, C., Wu, B., He, M., Xu, B., Wang, J., et al. (2023). Pangenomic analysis identifies structural variation associated with heat tolerance in pearl millet. Nat. Genet. *55*, 507–518. https://doi.org/10.1038/s41588-023-01302-4.

20. Gao, L., Gonda, I., Sun, H., Ma, Q., Bao, K., Tieman, D.M., Burzynski-Chang, E.A., Fish, T.L., Stromberg, K.A., Sacks, G.L., et al. (2019). The tomato pan-genome uncovers new genes and a rare allele regulating fruit flavor. Nat. Genet. *51*, 1044–1051. https://doi.org/10.1038/s41588-019-0410-2.

21. Yang, W., Duan, H., Yu, K., Hou, S., Kang, Y., Wang, X., Hao, J., Liu, L., Zhang, Y., Luo, L., et al. (2024). Integrative dissection of lignin composition in Tartary buckwheat seed hulls for enhanced dehulling efficiency. Adv. Sci. (Weinh) *11*, e2400916. https://doi.org/10.1002/advs.202400916.

22. Fawcett, J.A., Takeshima, R., Kikuchi, S., Yazaki, E., Katsube-Tanaka, T., Dong, Y., Li, M., Hunt, H.V., Jones, M.K., Lister, D.L., et al. (2023). Genome sequencing reveals the genetic architecture of heterostyly and domestication history of common buckwheat. Nat. Plants *9*, 1236–1251. https://doi.org/10.1038/s41477-023-01474-1.

23. Závodník, M., Fajkus, P., Franek, M., Kopecký, D., Garcia, S., Dodsworth, S., Orejuela, A., Kilar, A., Ptáček, J., Mátl, M., et al. (2023). Telomerase RNA gene paralogs in plants - the usual pathway to unusual telomeres. New Phytol. *239*, 2353–2366. https://doi.org/10.1111/nph.19110.

24. He, M., He, Y., Zhang, K., Lu, X., Zhang, X., Gao, B., Fan, Y., Zhao, H., Jha, R., Huda, M.N., et al. (2022). Comparison of buckwheat genomes reveals the genetic basis of metabolomic divergence and ecotype differentiation. New Phytol. *235*, 1927–1943. https://doi.org/10.1111/nph.18306.

25. Zhang, N., McHale, L.K., and Finer, J.J. (2019). Changes to the core and flanking sequences of G-box elements lead to increases and decreases in gene expression in both native and synthetic soybean promoters. Plant Biotechnol. J. *17*, 724–735. https://doi.org/10.1111/pbi.13010.

26. Chinnusamy, V., Ohta, M., Kanrar, S., Lee, B.H., Hong, X., Agarwal, M., and Zhu, J.K. (2003). ICE1: a regulator of cold-induced transcriptome and freezing tolerance in *Arabidopsis*. Genes Dev. *17*, 1043–1054. https://doi.org/10.1101/gad.1077503.

27. Li, W., Wen, Y., Quan, J., Gao, M., Shang, C., Liu, X., Liu, G., Hu, X., and Li, J. (2025). Regulation of jasmonic acid signalling in tomato cold stress response: Insights into the MYB15-LOXD and MYB15-MYC2-LOXD regulatory modules. Plant Biotechnol. J. *23*, 4246–4260. https://doi.org/10.1111/pbi.70201.

28. Liu, Y., Patra, B., Pattanaik, S., Wang, Y., and Yuan, L. (2019). GATA and phytochrome interacting factor transcription factors regulate light-induced vindoline biosynthesis in *Catharanthus roseus*. Plant Physiol. *180*, 1336–1350. https://doi.org/10.1104/pp.19.00489.

29. Wang, G., Xu, X., Lu, H., Mi, M., Qv, T., Shen, Y., Ran, J., Yang, D., Li, Y., Liu, T., et al. (2025). The bZIP transcription factor BcbZIP72 positively regulates cold tolerance through CBF-dependent pathways in non-heading Chinese cabbage. Plant Physiol. Biochem. *229*, 110522. https://doi.org/10.1016/j.plaphy.2025.110522.

30. Chen, S., Dong, X., Yang, Z., Hou, X., and Liu, L. (2021). Regulation of the development in *Physcomitrium* (*Physcomitrella*) patens implicates the functional differentiation of plant RNase H1s. Plant Sci. *313*, 111070. https://doi.org/10.1016/j.plantsci.2021.111070.

31. Cheng, L., Wang, W., Yao, Y., and Sun, Q. (2021). Mitochondrial RNase H1 activity regulates R-loop homeostasis to maintain genome integrity and enable early embryogenesis in *Arabidopsis*. PLoS Biol. *19*, e3001357. https://doi.org/10.1371/journal.pbio.3001357.

32. Kuciński, J., Chamera, S., Kmera, A., Rowley, M.J., Fujii, S., Khurana, P., Nowotny, M., and Wierzbicki, A.T. (2020). Evolutionary history and activity of RNase H1-like proteins in *Arabidopsis thaliana*. Plant Cell Physiol. *61*, 1107–1119. https://doi.org/10.1093/pcp/pcaa040.

33. Wang, W., Li, K., Yang, Z., Hou, Q., Zhao, W.W., and Sun, Q. (2021). RNase H1C collaborates with ssDNA binding proteins WHY1/3 and recombinase RecA1 to fulfill the DNA damage repair in *Arabidopsis* chloroplasts. Nucleic Acids Res. *49*, 6771–6787. https://doi.org/10.1093/nar/gkab479.

34. Yang, Z., Hou, Q., Cheng, L., Xu, W., Hong, Y., Li, S., and Sun, Q. (2017). RNase H1 cooperates with DNA gyrases to restrict R-loops and maintain genome integrity in *Arabidopsis* chloroplasts. Plant Cell *29*, 2478–2497. https://doi.org/10.1105/tpc.17.00305.

35. Hideg, E., Jansen, M.A.K., and Strid, A. (2013). UV-B exposure, ROS, and stress: inseparable companions or loosely linked associates? Trends Plant Sci. *18*, 107–115. https://doi.org/10.1016/j.tplants.2012.09.003.

36. Li, R., Chen, Z., Zheng, R., Chen, Q., Deng, J., Li, H., Huang, J., Liang, C., and Shi, T. (2023). QTL mapping and candidate gene analysis for yield and grain weight/size in Tartary buckwheat. BMC Plant Biol. *23*, 58. https://doi.org/10.1186/s12870-022-04004-x.

37. Li, J., Feng, S., Zhang, Y., Xu, L., Luo, Y., Yuan, Y., Yang, Q., and Feng, B. (2022). Genome-wide identification and expression analysis of the plant-specific *PLATZ* gene family in Tartary buckwheat (*Fagopyrum tataricum*). BMC Plant Biol. *22*, 160. https://doi.org/10.1186/s12870-022-03546-4.

38. Wang, A., Hou, Q., Si, L., Huang, X., Luo, J., Lu, D., Zhu, J., Shangguan, Y., Miao, J., Xie, Y., et al. (2019). The PLATZ transcription factor GL6 affects grain length and number in rice. Plant Physiol. *180*, 2077–2090. https://doi.org/10.1104/pp.18.01574.

39. Zhou, S.R., and Xue, H.W. (2020). The rice PLATZ protein SHORT GRAIN6 determines grain size by regulating spikelet hull cell division. J. Integr. Plant Biol. *62*, 847–864. https://doi.org/10.1111/jipb.12851.

40. Stratmann, J. (2003). Ultraviolet-B radiation co-opts defense signaling pathways. Trends Plant Sci. *8*, 526–533. https://doi.org/10.1016/j.tplants.2003.09.011.

41. Shi, C., and Liu, H. (2021). How plants protect themselves from ultraviolet-B radiation stress. Plant Physiol. *187*, 1096–1103. https://doi.org/10.1093/plphys/kiab245.

42. Liang, T., Shi, C., Peng, Y., Tan, H., Xin, P., Yang, Y., Wang, F., Li, X., Chu, J., Huang, J., et al. (2020). Brassinosteroid-activated BRI1-EMS-SUPPRESSOR 1 inhibits flavonoid biosynthesis and coordinates growth and UV-B stress responses in plants. Plant Cell *32*, 3224–3239. https://doi.org/10.1105/tpc.20.00048.

43. Hu, S., Chen, Y., Qian, C., Ren, H., Liang, X., Tao, W., Chen, Y., Wang, J., Dong, Y., Han, J., et al. (2024). Nuclear accumulation of rice UV-B photoreceptors is UV-B- and OsCOP1-independent for UV-B responses. Nat. Commun. *15*, 6396. https://doi.org/10.1038/s41467-024-50755-6.

44. Guo, H., Gao, S., Li, H., Yang, J., Li, J., Gu, Y., Lou, Q., Su, R., Ye, W., Zou, A., et al. (2025). Natural variation of *CTB5* confers cold adaptation in plateau *japonica* rice. Nat. Commun. *16*, 1032. https://doi.org/10.1038/s41467-025-56174-5.

45. Zeng, R., Shi, Y., Guo, L., Fu, D., Li, M., Zhang, X., Li, Z., Zhuang, J., Yang, X., Zuo, J., et al. (2025). A natural variant of *COOL1* gene enhances cold tolerance for high-latitude adaptation in maize. Cell *188*, 1315–1329.e13. https://doi.org/10.1016/j.cell.2024.12.018.

46. Shi, J., and Lai, J. (2015). Patterns of genomic changes with crop domestication and breeding. Curr. Opin. Plant Biol. *24*, 47–53. https://doi.org/10.1016/j.pbi.2015.01.008.

47. Tao, Y., Luo, H., Xu, J., Cruickshank, A., Zhao, X., Teng, F., Hathorn, A., Wu, X., Liu, Y., Shatte, T., et al. (2021). Extensive variation within the pan-

genome of cultivated and wild sorghum. Nat. Plants *7*, 766–773. https://doi.org/10.1038/s41477-021-00925-x.

48. He, Q., Tang, S., Zhi, H., Chen, J., Zhang, J., Liang, H., Alam, O., Li, H., Zhang, H., Xing, L., et al. (2023). A graph-based genome and pan-genome variation of the model plant *Setaria*. Nat. Genet. *55*, 1232–1242. https://doi.org/10.1038/s41588-023-01423-w.

49. Chen, J., Liu, Y., Liu, M., Guo, W., Wang, Y., He, Q., Chen, W., Liao, Y., Zhang, W., Gao, Y., et al. (2023). Pangenome analysis reveals genomic variations associated with domestication traits in broomcorn millet. Nat. Genet. *55*, 2243–2254. https://doi.org/10.1038/s41588-023-01571-z.

50. Wang, Y., Chen, W., Xing, M., Sun, J., Wang, S., Yang, Z., Huang, J., Nie, Y., Zhao, M., Li, Y., et al. (2024). Wild rice *GL12* synergistically improves grain length and salt tolerance in cultivated rice. Nat. Commun. *15*, 9453. https://doi.org/10.1038/s41467-024-53611-9.

51. Zhang, X., Meng, W., Liu, D., Pan, D., Yang, Y., Chen, Z., Ma, X., Yin, W., Niu, M., Dong, N., et al. (2024). Enhancing rice panicle branching and grain yield through tissue-specific brassinosteroid inhibition. Science *383*, eadk8838. https://doi.org/10.1126/science.adk8838.

52. Zsögön, A., Čermák, T., Naves, E.R., Notini, M.M., Edel, K.H., Weinl, S., Freschi, L., Voytas, D.F., Kudla, J., and Peres, L.E.P. (2018). *De novo* domestication of wild tomato using genome editing. Nat. Biotechnol. *36*, 1211–1216. https://doi.org/10.1038/nbt.4272.

53. Yu, H., Lin, T., Meng, X., Du, H., Zhang, J., Liu, G., Chen, M., Jing, Y., Kou, L., Li, X., et al. (2021). A route to *de novo* domestication of wild allotetraploid rice. Cell *184*, 1156–1170.e14. https://doi.org/10.1016/j.cell.2021.01.013.

54. Cheng, H., Jarvis, E.D., Fedrigo, O., Koepfli, K.P., Urban, L., Gemmell, N.J., and Li, H. (2022). Haplotype-resolved assembly of diploid genomes without parental data. Nat. Biotechnol. *40*, 1332–1335. https://doi.org/10.1038/s41587-022-01261-x.

55. Zhang, H., Song, L., Wang, X., Cheng, H., Wang, C., Meyer, C.A., Liu, T., Tang, M., Aluru, S., Yue, F., et al. (2021). Fast alignment and preprocessing of chromatin profiles with Chromap. Nat. Commun. *12*, 6566. https://doi.org/10.1038/s41467-021-26865-w.

56. Zhou, C., McCarthy, S.A., and Durbin, R. (2023). YaHS: yet another Hi-C scaffolding tool. Bioinformatics *39*, btac808. https://doi.org/10.1093/bioinformatics/btac808.

57. Manni, M., Berkeley, M.R., Seppey, M., Simão, F.A., and Zdobnov, E.M. (2021). BUSCO update: novel and streamlined workflows along with broader and deeper phylogenetic coverage for scoring of eukaryotic, prokaryotic, and viral genomes. Mol. Biol. Evol. *38*, 4647–4654. https://doi.org/10.1093/molbev/msab199.

58. Ou, S., Su, W., Liao, Y., Chougule, K., Agda, J.R.A., Hellinga, A.J., Lugo, C.S.B., Elliott, T.A., Ware, D., Peterson, T., et al. (2019). Benchmarking transposable element annotation methods for creation of a streamlined, comprehensive pipeline. Genome Biol. *20*, 275. https://doi.org/10.1186/s13059-019-1905-y.

59. Birney, E., Clamp, M., and Durbin, R. (2004). Genewise and genomewise. Genome Res. *14*, 988–995. https://doi.org/10.1101/gr.1865504.

60. Stanke, M., Steinkamp, R., Waack, S., and Morgenstern, B. (2004). AUGUSTUS: a web server for gene finding in eukaryotes. Nucleic Acids Res. *32*, W309–W312. https://doi.org/10.1093/nar/gkh379.

61. Majoros, W.H., Pertea, M., and Salzberg, S.L. (2004). TigrScan and GlimmerHMM: two open source ab initio eukaryotic gene-finders. Bioinformatics *20*, 2878–2879. https://doi.org/10.1093/bioinformatics/bth315.

62. Kim, D., Paggi, J.M., Park, C., Bennett, C., and Salzberg, S.L. (2019). Graph-based genome alignment and genotyping with HISAT2 and HISAT-genotype. Nat. Biotechnol. *37*, 907–915. https://doi.org/10.1038/s41587-019-0201-4.

63. Haas, B.J., Delcher, A.L., Mount, S.M., Wortman, J.R., Smith, R.K., Jr., Hannick, L.I., Maiti, R., Ronning, C.M., Rusch, D.B., Town, C.D., et al. (2003). Improving the Arabidopsis genome annotation using maximal transcript alignment assemblies. Nucleic Acids Res. *31*, 5654–5666. https://doi.org/10.1093/nar/gkg770.

64. Haas, B.J., Salzberg, S.L., Zhu, W., Pertea, M., Allen, J.E., Orvis, J., White, O., Buell, C.R., and Wortman, J.R. (2008). Automated eukaryotic gene structure annotation using EVidenceModeler and the program to assemble spliced alignments. Genome Biol. *9*, R7. https://doi.org/10.1186/gb-2008-9-1-r7.

65. Lin, Y., Ye, C., Li, X., Chen, Q., Wu, Y., Zhang, F., Pan, R., Zhang, S., Chen, S., Wang, X., et al. (2023). quarTeT: a telomere-to-telomere toolkit for gap-free genome assembly and centromeric repeat identification. Hortic. Res. *10*, uhad127. https://doi.org/10.1093/hr/uhad127.

66. Tang, H., Krishnakumar, V., Zeng, X., Xu, Z., Taranto, A., Lomas, J.S., Zhang, Y., Huang, Y., Wang, Y., Yim, W.C., et al. (2024). JCVI: A versatile toolkit for comparative genomics analysis. Imeta *3*, e211. https://doi.org/10.1002/imt2.211.

67. Shen, W., Sipos, B., and Zhao, L. (2024). SeqKit2: A Swiss army knife for sequence and alignment processing. Imeta *3*, e191. https://doi.org/10.1002/imt2.191.

68. Chao, K.H., Heinz, J.M., Hoh, C., Mao, A., Shumate, A., Pertea, M., and Salzberg, S.L. (2025). Combining DNA and protein alignments to improve genome annotation with LiftOn. Genome Res. *35*, 311–325. https://doi.org/10.1101/gr.279620.124.

69. Andrews S. (2010). FastQC: a quality control tool for high throughput sequence data. Babraham Bioinfomatics. https://www.bioinformatics.babraham.ac.uk/projects/fastqc/.

70. Bolger, A.M., Lohse, M., and Usadel, B. (2014). Trimmomatic: a flexible trimmer for Illumina sequence data. Bioinformatics *30*, 2114–2120. https://doi.org/10.1093/bioinformatics/btu170.

71. Langmead, B., and Salzberg, S.L. (2012). Fast gapped-read alignment with Bowtie 2. Nat. Methods *9*, 357–359. https://doi.org/10.1038/nmeth.1923.

72. Li, H., Handsaker, B., Wysoker, A., Fennell, T., Ruan, J., Homer, N., Marth, G., Abecasis, G., and Durbin, R.; 1000 Genome Project Data Processing Subgroup (2009). The sequence alignment/map format and SAMtools. Bioinformatics *25*, 2078–2079. https://doi.org/10.1093/bioinformatics/btp352.

73. McKenna, A., Hanna, M., Banks, E., Sivachenko, A., Cibulskis, K., Kernytsky, A., Garimella, K., Altshuler, D., Gabriel, S., Daly, M., et al. (2010). The genome analysis Toolkit: a mapreduce framework for analyzing next-generation DNA sequencing data. Genome Res. *20*, 1297–1303. https://doi.org/10.1101/gr.107524.110.

74. Zhang, Y., Liu, T., Meyer, C.A., Eeckhoute, J., Johnson, D.S., Bernstein, B.E., Nusbaum, C., Myers, R.M., Brown, M., Li, W., et al. (2008). Model-based analysis of ChIP-Seq (MACS). Genome Biol. *9*, R137. https://doi.org/10.1186/gb-2008-9-9-r137.

75. Vasimuddin, M., Misra, S., Li, H., and Aluru, S. (2019). Efficient architecture-aware acceleration of BWA-MEM for multicore systems. In IPDPS (Institute of Electrical and Electronics Engineers), pp. 314–324. https://doi.org/10.1109/IPDPS.2019.00041.

76. Wang, K., Li, M., and Hakonarson, H. (2010). ANNOVAR: functional annotation of genetic variants from high-throughput sequencing data. Nucleic Acids Res. *38*, e164. https://doi.org/10.1093/nar/gkq603.

77. Purcell, S., Neale, B., Todd-Brown, K., Thomas, L., Ferreira, M.A.R., Bender, D., Maller, J., Sklar, P., de Bakker, P.I.W., Daly, M.J., et al. (2007). PLINK: a tool set for whole-genome association and population-based linkage analyses. Am. J. Hum. Genet. *81*, 559–575. https://doi.org/10.1086/519795.

78. Vilella, A.J., Severin, J., Ureta-Vidal, A., Heng, L., Durbin, R., and Birney, E. (2009). Ensemblcompara genetrees: complete, duplication-aware phylogenetic trees in vertebrates. Genome Res. *19*, 327–335. https://doi.org/10.1101/gr.073585.107.

79. Letunic, I., and Bork, P. (2021). Interactive Tree Of Life (iTOL) v5: an online tool for phylogenetic tree display and annotation. Nucleic Acids Res. *49*, W293–W296. https://doi.org/10.1093/nar/gkab301.

80. Alexander, D.H., Novembre, J., and Lange, K. (2009). Fast model-based estimation of ancestry in unrelated individuals. Genome Res. *19*, 1655–1664. https://doi.org/10.1101/gr.094052.109.

81. Yang, J., Lee, S.H., Goddard, M.E., and Visscher, P.M. (2011). GCTA: a tool for genome-wide complex trait analysis. Am. J. Hum. Genet. *88*, 76–82. https://doi.org/10.1016/j.ajhg.2010.11.011.

82. Zhang, C., Dong, S.S., Xu, J.Y., He, W.M., and Yang, T.L. (2019). PopLDdecay: a fast and effective tool for linkage disequilibrium decay analysis based on variant call format files. Bioinformatics *35*, 1786–1788. https://doi.org/10.1093/bioinformatics/bty875.

83. Buchfink, B., Xie, C., and Huson, D.H. (2015). Fast and sensitive protein alignment using DIAMOND. Nat. Methods *12*, 59–60. https://doi.org/10.1038/nmeth.3176.

84. Emms, D.M., and Kelly, S. (2015). OrthoFinder: solving fundamental biases in whole genome comparisons dramatically improves orthogroup inference accuracy. Genome Biol. *16*, 157. https://doi.org/10.1186/s13059-015-0721-2.

85. Edgar, R.C. (2004). MUSCLE: a multiple sequence alignment method with reduced time and space complexity. BMC Bioinform. *5*, 113. https://doi.org/10.1186/1471-2105-5-113.

86. Wu, T., Hu, E., Xu, S., Chen, M., Guo, P., Dai, Z., Feng, T., Zhou, L., Tang, W., Zhan, L., et al. (2021). clusterProfiler 4.0: A universal enrichment tool for interpreting omics data. Innovation (Camb.) *2*, 100141. https://doi.org/10.1016/j.xinn.2021.100141.

87. Sun, P., Jiao, B., Yang, Y., Shan, L., Li, T., Li, X., Xi, Z., Wang, X., and Liu, J. (2022). WGDI: A user-friendly toolkit for evolutionary analyses of whole-genome duplications and ancestral karyotypes. Mol. Plant *15*, 1841–1851. https://doi.org/10.1016/j.molp.2022.10.018.

88. Marçais, G., Delcher, A.L., Phillippy, A.M., Coston, R., Salzberg, S.L., and Zimin, A. (2018). MUMmer4: A fast and versatile genome alignment system. PLOS Comput. Biol. *14*, e1005944. https://doi.org/10.1371/journal.pcbi.1005944.

89. Goel, M., Sun, H., Jiao, W.B., and Schneeberger, K. (2019). SyRI: finding genomic rearrangements and local sequence differences from whole-genome assemblies. Genome Biol. *20*, 277. https://doi.org/10.1186/s13059-019-1911-0.

90. Jeffares, D.C., Jolly, C., Hoti, M., Speed, D., Shaw, L., Rallis, C., Balloux, F., Dessimoz, C., Bähler, J., and Sedlazeck, F.J. (2017). Transient structural variations have strong effects on quantitative traits and reproductive isolation in fission yeast. Nat. Commun. *8*, 14061. https://doi.org/10.1038/ncomms14061.

91. Garrison, E., Sirén, J., Novak, A.M., Hickey, G., Eizenga, J.M., Dawson, E.T., Jones, W., Garg, S., Markello, C., Lin, M.F., et al. (2018). Variation graph toolkit improves read mapping by representing genetic variation in the reference. Nat. Biotechnol. *36*, 875–879. https://doi.org/10.1038/nbt.4227.

92. Chen, H., Patterson, N., and Reich, D. (2010). Population differentiation as a test for selective sweeps. Genome Res. *20*, 393–402. https://doi.org/10.1101/gr.100545.109.

93. Jones, P., Binns, D., Chang, H.Y., Fraser, M., Li, W., McAnulla, C., McWilliam, H., Maslen, J., Mitchell, A., Nuka, G., et al. (2014). InterProScan 5: genome-scale protein function classification. Bioinformatics *30*, 1236–1240. https://doi.org/10.1093/bioinformatics/btu031.

94. Katoh, K., and Standley, D.M. (2013). MAFFT multiple sequence alignment software version 7: improvements in performance and usability. Mol. Biol. Evol. *30*, 772–780. https://doi.org/10.1093/molbev/mst010.

95. Capella-Gutiérrez, S., Silla-Martínez, J.M., and Gabaldón, T. (2009). trimAl: a tool for automated alignment trimming in large-scale phylogenetic analyses. Bioinformatics *25*, 1972–1973. https://doi.org/10.1093/bioinformatics/btp348.

96. Nguyen, L.T., Schmidt, H.A., von Haeseler, A., and Minh, B.Q. (2015). IQ-TREE: a fast and effective stochastic algorithm for estimating maximum-likelihood phylogenies. Mol. Biol. Evol. *32*, 268–274. https://doi.org/10.1093/molbev/msu300.

97. Zhou, X., and Stephens, M. (2012). Genome-wide efficient mixed-model analysis for association studies. Nat. Genet. *44*, 821–824. https://doi.org/10.1038/ng.2310.

98. Chen, S., Zhou, Y., Chen, Y., and Gu, J. (2018). fastp: an ultra-fast all-in-one FASTQ preprocessor. Bioinformatics *34*, i884–i890. https://doi.org/10.1093/bioinformatics/bty560.

99. Liao, Y., Smyth, G.K., and Shi, W. (2014). featureCounts: an efficient general purpose program for assigning sequence reads to genomic features. Bioinformatics *30*, 923–930. https://doi.org/10.1093/bioinformatics/btt656.

100. Love, M.I., Huber, W., and Anders, S. (2014). Moderated estimation of fold change and dispersion for RNA-seq data with DESeq2. Genome Biol. *15*, 550. https://doi.org/10.1186/s13059-014-0550-8.

101. Kaufmann, K., Muiño, J.M., Østerås, M., Farinelli, L., Krajewski, P., and Angenent, G.C. (2010). Chromatin immunoprecipitation (ChIP) of plant transcription factors followed by sequencing (ChIP-SEQ) or hybridization to whole genome arrays (ChIP-CHIP). Nat. Protoc. *5*, 457–472. https://doi.org/10.1038/nprot.2009.244.

102. Tang, S.Y., Tang, Z.X., Qiu, L., Yang, Z.J., Li, G.R., Lang, T., Zhu, W.Q., Zhang, J.H., and Fu, S.L. (2018). Developing new oligo probes to distinguish specific chromosomal segments and the A, B, D genomes of wheat (*Triticum aestivum* L.) using ND-FISH. Front. Plant Sci. *9*, 1104. https://doi.org/10.3389/fpls.2018.01104.

103. Liu, Y., Du, H., Li, P., Shen, Y., Peng, H., Liu, S., Zhou, G.A., Zhang, H., Liu, Z., Shi, M., et al. (2020). Pan-genome of wild and cultivated soybeans. Cell *182*, 162–176.e13. https://doi.org/10.1016/j.cell.2020.05.023.

104. Kalyaanamoorthy, S., Minh, B.Q., Wong, T.K.F., von Haeseler, A., and Jermiin, L.S. (2017). ModelFinder: fast model selection for accurate phylogenetic estimates. Nat. Methods *14*, 587–589. https://doi.org/10.1038/nmeth.4285.

105. Hoang, D.T., Chernomor, O., von Haeseler, A., Minh, B.Q., and Vinh, L.S. (2018). UFBoot2: improving the ultrafast bootstrap approximation. Mol. Biol. Evol. *35*, 518–522. https://doi.org/10.1093/molbev/msx281.

106. Pinski, A., and Betekhtin, A. (2023). Efficient Agrobacterium-mediated transformation and genome editing of *Fagopyrum tataricum*. Front. Plant Sci. *14*, 1270150. https://doi.org/10.3389/fpls.2023.1270150.

107. Wang, X., Prokhnevsky, A.I., Skarjinskaia, M., Razzak, M.A., Streatfield, S.J., and Lee, J.Y. (2023). Facilitating viral vector movement enhances heterologous protein production in an established plant system. Plant Biotechnol. J. *21*, 635–645. https://doi.org/10.1111/pbi.13977.

108. Hiei, Y., Ohta, S., Komari, T., and Kumashiro, T. (1994). Efficient transformation of rice (*Oryza sativa* L.) mediated by *Agrobacterium* and sequence analysis of the boundaries of the T-DNA. Plant J. *6*, 271–282. https://doi.org/10.1046/j.1365-313x.1994.6020271.x.

109. Xie, Y., Miao, T., Lyu, S., Huang, Y., Shu, M., Li, S., and Xiong, T. (2024). *Arabidopsis* ERD15 regulated by BBX24 plays a positive role in UV-B signaling. Plant Sci. *343*, 112077. https://doi.org/10.1016/j.plantsci.2024.112077.

110. He, J., Hao, Y., He, Y., Li, W., Shi, Y., Khurshid, M., Lai, D., Ma, C., Wang, X., Li, J., et al. (2024). Genome-wide associated study identifies *FtPMEI13* gene conferring drought resistance in Tartary buckwheat. Plant J. *120*, 2398–2419. https://doi.org/10.1111/tpj.17119.

111. Sun, Q., Csorba, T., Skourti-Stathaki, K., Proudfoot, N.J., and Dean, C. (2013). R-loop stabilization represses antisense transcription at the *Arabidopsis* FLC locus. Science *340*, 619–621. https://doi.org/10.1126/science.1234848.

112. Yang, X., Zhang, W., Dong, M., Boubriak, I., and Huang, Z. (2011). The achene mucilage hydrated in desert dew assists seed cells in maintaining DNA integrity: adaptive strategy of desert plant *Artemisia sphaerocephala*. PLoS One *6*, e24346. https://doi.org/10.1371/journal.pone.0024346.

113. Wang, Z., Gao, M., Li, Y., Zhang, J., Su, H., Cao, M., Liu, Z., Zhang, X., Zhao, B., Guo, Y.D., et al. (2022). The transcription factor SlWRKY37 positively regulates jasmonic acid- and dark-induced leaf senescence in tomato. J. Exp. Bot. *73*, 6207–6225. https://doi.org/10.1093/jxb/erac258.

Please cite this article in press as: Zhang et al., Pangenome-guided breeding restores high-altitude adaptation and improves yield in Tartary buckwheat, Cell (2026), https://doi.org/10.1016/j.cell.2026.07.035

CellPress

STAR★METHODS

KEY RESOURCES TABLE

REAGENT or RESOURCE	SOURCE	IDENTIFIER
Antibodies		
Anti-CENH3 antibody	Abcam	Cat# ab72001
Goat Anti-Rabbit IgG Antibody	Sigma-Aldrich	Cat# AP132; RRID: AB_11214051
Anti-RNA:DNA hybrid antibody S9.6	Sigma-Aldrich	Cat# MABE1095; RRID: AB_2861387
HRP-conjugated Goat Anti-Mouse IgG	Cwbiotech	Cat# CW0102S; RRID: AB_2736997
Anti-phospho-Histone H2A.X (Ser139) Antibody	Millipore	Cat# 05-636; RRID: AB_309864
Donkey anti-Sheep IgG (H+L) Cross-Adsorbed Secondary Antibody, Alexa Fluor™ Plus 488	Thermo Fisher Scientific	Cat# A11015; RRID: AB_2534082
Bacterial and virus strains		
Agrobacterium tumefaciens strain GV3101	Weidi Biotechnology	Cat# AC1001
Agrobacterium tumefaciens GV3101 (pSoup-p19)	Weidi Biotechnology	Cat# AC1003
Escherichia coli BL21 (DE3)	Weidi Biotechnology	Cat# EC1002
Yeast strain Y2HGold	Weidi Biotechnology	Cat# YC1002
Chemicals, peptides, and recombinant proteins		
Cetyltrimethylammonium bromide (CTAB)	Coolaber	Cat# CC3991
RNase A	Vazyme	Cat# DE111
Proteinase K	Invitrogen	Cat# 25530049
DynaGreen™ Protein A/G beads	Invitrogen	Cat# 80105G
VAHTS DNA Clean Beads	Vazyme	Cat# N411
GST•Bind™ Resin	Millipore	Cat# 70541
HaloTag Beads	Promega	Cat# G7281
Formaldehyde	Sigma-Aldrich	Cat# F8775
PMSF	Sigma-Aldrich	Cat# 93482
Complete protease inhibitor cocktail	Roche	Cat# 4693116001
Hygromycin B	Coolaber	Cat# CH6361
IPTG	Coolaber	Cat# SL3861
Propidium iodide (PI)	Coolaber	Cat# CP9161
DAPI	Solarbio	Cat# C0060
Toluidine blue	Yuanye	Cat# S19058
Potassium luciferin	Coolaber	Cat# CL6930
Recombinant FtRNH-His protein (Hap1)	This study	N/A
Recombinant FtRNH-His protein (Hap2)	This study	N/A
Recombinant FtPLATZ3-GST fusion protein	This study	N/A
Recombinant FtPLATZ3-Halo fusion protein	This study	N/A
His-tagged empty protein (control)	This study	N/A
GST-tagged empty protein (control)	This study	N/A
Critical commercial assays		
HiScript III RT SuperMix for RT-qPCR	Vazyme	Cat# R323-01
Polysaccharide and Polyphenol Plant Total RNA Extraction Kit	Tiangen	Cat# DP441

(*Continued on next page*)

Please cite this article in press as: Zhang et al., Pangenome-guided breeding restores high-altitude adaptation and improves yield in Tartary buckwheat, Cell (2026), https://doi.org/10.1016/j.cell.2026.07.035

Continued

REAGENT or RESOURCE	SOURCE	IDENTIFIER
TruePrep DNA Library Prep Kit V2 for Illumina	Vazyme	Cat# TD501
OxiSelect™ UV-Induced DNA Damage ELISA Kit (CPDs and 6-4PPs)	Cell Biolabs	Cat# STA-322-C
Tetramethyl-Rhodamine (TMR, Red) TUNEL Cell Apoptosis Detection Kit	Servicebio	Cat# G1502
LightShift Chemiluminescent EMSA Kit	Thermo Fisher Scientific	Cat# 20148X
TNT SP6 High-Yield Wheat Germ Protein Expression System	Promega	Cat# L3260
StarPrep Gel Extraction Kit	Genstar	Cat# D205
Hieff® Smearase	Yeasen	Cat# 12907ES24
Deposited data		
PacBio CCS, ONT, Hi-C, and other sequencing data	This study	BioProject: PRJCA036855
Genome assemblies	This study	https://figshare.com/s/754ddf20dcf4455056c7
Public buckwheat genome assemblies	He et al.[2]; Lin et al.[14]; Du et al.[17]	N/A
Public buckwheat whole-genome sequencing data	He et al.[2]; Zhang et al.[3]	N/A
Experimental models: Organisms/strains		
Fagopyrum tataricum cv. ZK3	This study	N/A
Fagopyrum tataricum accession XZ751	This study	N/A
Fagopyrum tataricum accession XZ625	This study	N/A
Fagopyrum tataricum accession HB91	This study	N/A
NIL-*FtRNH*^{Hap1}	This study	N/A
NIL-*FtRNH*^{Hap2}	This study	N/A
NIL-*FtPLATZ3*^{Hap2}	This study	N/A
NIL-*FtRNH*^{Hap2}-*FtPLATZ3*^{Hap2}	This study	N/A
NIL-*FtRNH*^{Hap2}-*FtPLATZ3*^{Hap2}-MC	This study	N/A
Arabidopsis thaliana (*Col-0*)	Laboratory stock	N/A
FtRNH-overexpressing *Arabidopsis* lines	This study	N/A
FtPLATZ3-overexpressing *Arabidopsis* lines	This study	N/A
Oryza sativa cv. *ZH11*	Laboratory stock	N/A
FtRNH-overexpressing rice lines	This study	N/A
FtPLATZ3-overexpressing rice lines	This study	N/A
Nicotiana benthamiana	Laboratory stock	N/A
FtPLATZ3-overexpressing Tartary buckwheat lines	This study	N/A
FtPLATZ3 knockout Tartary buckwheat lines	This study	N/A
FtRNH-overexpressing Tartary buckwheat lines	This study	N/A
FtRNH mutant Tartary buckwheat lines	This study	N/A
Oligonucleotides		
See Table S5A	This study	N/A
Recombinant DNA		
pCAMBIA-1307	Novopro	Cat# V041077
pCAMBIA-1302	Novopro	Cat# V010892
p2300-35S-H2B-mCherry	This study	N/A

(*Continued on next page*)

Continued

REAGENT or RESOURCE	SOURCE	IDENTIFIER
pGreenII 0800-LUC	Novopro	Cat# V010545
pGreenII 62SK	Novopro	Cat# V012539
pCAMBIA1301UbiNOS	This study	N/A
pGEX-4T-1	Novopro	Cat# V010918
pGBKT7	Clontech	Cat# 630443
pGADT7	Clontech	Cat# 630442
FtRNH-pCAMBIA1307	This study	N/A
FtPLATZ3-pCAMBIA1307	This study	N/A
FtRNH-pCAMBIA1305-GFP	This study	N/A
FtPLATZ3-pCAMBIA1302-GFP	This study	N/A
FtPLATZ3-pGEX-4T-1	This study	N/A
FtPLATZ3-Halo	This study	N/A
FtRNH-p1301UbiNOS	This study	N/A
FtPLATZ3-p1301UbiNOS	This study	N/A
FtPLATZ3 promoter (Hap1)-pGreenII 0800-LUC	This study	N/A
FtPLATZ3 promoter (Hap2)-pGreenII 0800-LUC	This study	N/A
FtPLATZ3 promoter (Hap2–28bp)-pGreenII 0800-LUC	This study	N/A
FtPLATZ3 promoter (Hap1+28bp)-pGreenII 0800-LUC	This study	N/A
FtPLATZ3 promoter (Hap2 MYB/Dof mutant)-pGreenII 0800-LUC	This study	N/A
FtPLATZ3 CDS-pGreenII 62SK	This study	N/A
FtCYC promoter-pGreenII 0800-LUC	This study	N/A
FtEXP1 promoter-pGreenII 0800-LUC	This study	N/A
FtRPC53a-pGBKT7	This study	N/A
FtTFC1-pGBKT7	This study	N/A
Software and algorithms		
hifiasm (v0.18.9-r527)	Cheng et al.[54]	https://github.com/chhylp123/hifiasm
Chromap (v0.2.4-r467)	Zhang et al.[55]	https://github.com/haowenz/chromap
YaHS (v1.2a.1)	Zhou et al.[56]	https://github.com/c-zhou/yahs
BUSCO (v5.4.6)	Manni et al.[57]	https://busco.ezlab.org/
EDTA (v2.1.0)	Ou et al.[58]	https://github.com/oushujun/EDTA
GeneWise (WISE2 v2.4.1)	Birney et al.[59]	https://www.ebi.ac.uk/~birney/wise2/
Augustus (v3.5.0)	Stanke et al.[60]	https://bioinf.uni-greifswald.de/augustus/
GlimmerHMM (v3.0.1)	Majoros et al.[61]	https://ccb.jhu.edu/software/glimmerhmm/
HISAT2 (v2.1.0)	Kim et al.[62]	https://daehwankimlab.github.io/hisat2/
PASA (v2.5.3)	Haas et al.[63]	https://github.com/PASApipeline/PASApipeline
EVidenceModeler (v2.1.0)	Haas et al.[64]	https://evidencemodeler.github.io/
quarTeT (v1.1.5)	Lin et al.[65]	https://github.com/aaranyue/quarTeT
JCVI / MCScan (v1.4.23)	Tang et al.[66]	https://github.com/tanghaibao/jcvi
SeqKit (v2.8.2)	Shen et al.[67]	https://bioinf.shenwei.me/seqkit/
LiftOn (v1.0.4)	Chao et al.[68]	https://github.com/nextgenusfs/LiftOn
FastQC (v0.12.1)	Andrews[69]	https://www.bioinformatics.babraham.ac.uk/projects/fastqc/
Trimmomatic (v0.33)	Bolger et al.[70]	http://www.usadellab.org/cms/?page=trimmomatic

(*Continued on next page*)

Please cite this article in press as: Zhang et al., Pangenome-guided breeding restores high-altitude adaptation and improves yield in Tartary buckwheat, Cell (2026), https://doi.org/10.1016/j.cell.2026.07.035

Continued

REAGENT or RESOURCE	SOURCE	IDENTIFIER
Bowtie2 (v2.5.4)	Langmead & Salzberg[71]	https://bowtie-bio.sourceforge.net/bowtie2/
SAMtools (v1.17)	Li et al.[72]	http://www.htslib.org/
GATK (v4.2.2.0)	McKenna et al.[73]	https://gatk.broadinstitute.org/
MACS3 (v3.0.2)	Zhang et al.[74]	https://github.com/macs3-project/MACS
BWA-MEM2 (v2.2.1)	Vasimuddin et al.[75]	https://github.com/bwa-mem2/bwa-mem2
ANNOVAR (v2013-05-20)	Wang et al.[76]	https://annovar.openbioinformatics.org/
PLINK (v1.9)	Purcell et al.[77]	https://www.cog-genomics.org/plink/
TreeBest (v1.9.2)	Vilella et al.[78]	https://github.com/Ensembl/treebest
iTOL	Letunic & Bork[79]	https://itol.embl.de/
ADMIXTURE (v1.23)	Alexander et al.[80]	https://dalexander.github.io/admixture/
GCTA (v1.94.1)	Yang et al.[81]	https://yanglab.westlake.edu.cn/software/gcta/
PopLDdecay (v3.41)	Zhang et al.[82]	https://github.com/BGI-shenzhen/PopLDdecay
DIAMOND (v2.1.4.158)	Buchfink et al.[83]	https://github.com/bbuchfink/diamond
OrthoFinder (v2.5.5)	Emms & Kelly[84]	https://github.com/davidemms/OrthoFinder
MUSCLE (v3.7)	Edgar[85]	https://www.drive5.com/muscle/
clusterProfiler (v4.8.3)	Wu et al.[86]	https://bioconductor.org/packages/clusterProfiler/
WGDI (v0.6.5)	Sun et al.[87]	https://github.com/SunPengChuan/wgdi
MUMmer4 (v4.0.1)	Marçais et al.[88]	https://github.com/mummer4/mummer
SyRI (v1.7.1)	Goel et al.[89]	https://github.com/schneebergerlab/syri
SURVIVOR (v1.0.7)	Jeffares et al.[90]	https://github.com/fritzsedlazeck/SURVIVOR
vg toolkit (v1.53.0)	Garrison et al.[91]	https://github.com/vgteam/vg
XP-CLR (v1.1)	Chen et al.[92]	https://github.com/hardingnj/xpclr
InterProScan	Jones et al.[93]	https://www.ebi.ac.uk/interpro/
MAFFT (v7.520)	Katoh & Standley[94]	https://mafft.cbrc.jp/alignment/software/
trimAl (v1.4.rev15)	Capella-Gutiérrez et al.[95]	http://trimal.cgenomics.org/
IQ-TREE (v2.2.2.3)	Nguyen et al.[96]	http://www.iqtree.org/
GEMMA (v0.96)	Zhou & Stephens[97]	https://github.com/genetics-statistics/GEMMA
fastp (v1.1.0)	Chen et al.[98]	https://github.com/OpenGene/fastp
featureCounts (v2.0.3)	Liao et al.[99]	https://subread.sourceforge.net/
DESeq2 (v1.38.3)	Love et al.[100]	https://bioconductor.org/packages/DESeq2/

EXPERIMENTAL MODEL AND STUDY PARTICIPANT DETAILS

Tartary buckwheat (*Fagopyrum tataricum*)

A global diversity panel of 994 accessions from 15 countries was used, comprising 580 accessions reported in previous studies[2,3] and 414 newly collected accessions (see Table S1H for details). ZK3 (ZHONGKU NO. 3) was used for T2T reference genome assembly and served as the genetic background for near-isogenic line development. For pangenome construction, 16 accessions were selected, including ZK3, three previously published genomes,[2,14,17] and 12 newly assembled genomes representing the HW, SL, and NL groups. EMS mutants of *FtRNH* were generated in the wild accession XZ751 background. Knockout of the insertion in the *FtPLATZ3* promoter was performed in the HB91 background. All other transgenic overexpression and CRISPR-Cas9 knockout lines were produced in the K3 background. Near-isogenic lines (NILs) were developed in the ZK3 background: NIL-*FtRNH*^{Hap1} (donor XZ751), NIL-*FtRNH*^{Hap2} (donor XZ625), NIL-*FtPLATZ3*^{Hap2} (donor HB91), and NIL-*FtRNH*^{Hap2}-*FtPLATZ3*^{Hap2}. An improved line, NIL-*FtRNH*^{Hap2}-*FtPLATZ3*^{Hap2}-MC (more copy), carrying additional *FtPLATZ* copies, was generated by unequal recombination crossing and backcrossing.

Please cite this article in press as: Zhang et al., Pangenome-guided breeding restores high-altitude adaptation and improves yield in Tartary buckwheat, Cell (2026), https://doi.org/10.1016/j.cell.2026.07.035

Other experimental models

Wild-type *Arabidopsis thaliana* (*Col-0*), *Oryza sativa* cv. ZH11, *Nicotiana benthamiana*, *Agrobacterium tumefaciens* strain GV3101, *Escherichia coli* strain BL21 (DE3), and *Saccharomyces cerevisiae* strain Y2HGold were obtained from laboratory stocks. Transgenic lines overexpressing *FtRNH* or *FtPLATZ3* were generated in the *Col-0* and ZH11 backgrounds, respectively.

METHOD DETAILS

DNA extraction

Healthy leaves were harvested and immediately frozen in liquid nitrogen. Genomic DNA was extracted using a modified cetyltrimethylammonium bromide (CTAB) method. RNase A (Vazyme) was used to remove RNA contamination, and DNA quality was assessed by 1.5% agarose gel electrophoresis.

Genome sequencing, assembly, and quality assessment

Accessions used for genome assembly were grown at the Chinese Academy of Agricultural Sciences in Beijing, China. For PacBio sequencing, a 15-Kb SMRTbell library was prepared from genomic DNA according to the manufacturer's guidelines and sequenced on the PacBio Sequel II platform. Subreads were processed using CCS software with default settings to generate long (~15 Kb) and highly accurate (99%) HiFi reads. For Oxford Nanopore Technologies (ONT) ultra-long DNA sequencing, a library was prepared from high-quality DNA lightly fragmented to preserve >100 Kb lengths, following the standard ultra-long library construction protocol. To generate the primary contig set, we assembled the HiFi reads using hifiasm (v0.18.9-r527),[54] integrating the ONT ultra-long reads via the –ul parameter to resolve complex repeat regions and close gaps. Hi-C data were employed to anchor contigs, further enhancing assembly quality. Clean reads were aligned to the assembled genome using Chromap (v0.2.4-r467).[55] YaHS (v1.2a.1)[56] was used for correction, clustering, and orientation of the contigs. The integration of HiFi, ONT, and Hi-C data resulted in eight large contigs representing the eight chromosomes of ZK3. We applied the same method to obtain HiFi reads for 12 Tartary buckwheat individuals. Contigs were assembled using the default parameters of hifiasm (v0.18.9-r527). Subsequently, following the same strategy as ZK3, the contigs of these individuals were anchored to the chromosome level using their respective Hi-C data. Genome completeness was evaluated using BUSCO (v5.4.6)[57] with the single-copy orthologs from the embryophyta_odb10.2019-11-20 database. Genome continuity was assessed by calculating the contig N50 length. Additionally, the assembled genome was evaluated using the LTR Assembly Index (LAI).

Genome annotation

The prediction of repeat sequences in the genome was performed using the EDTA pipeline (v2.1.0)[58] with the parameters –step all –sensitive 1 –anno 1. Within this pipeline, LTR retrotransposons were identified using LTRharvest, LTR_FINDER, and LTR_retriever. Generic Repeat Finder and TIR-Learner were employed to predict TIR transposons, while HelitronScanner was used for the prediction of Helitron transposons.

For the prediction of high-quality protein-coding genes, we used a combination of homology-based, transcriptome-based, and *de novo* approaches. Homology-based prediction involved using protein sequences from the previously published *Fagopyrum tataricum* (Pinku1) genome with GeneWise (WISE2 v2.4.1).[59] For *ab initio* gene prediction, we used Augustus (v3.5.0)[60] and GlimmerHMM (v3.0.1).[61] Transcriptome-based prediction was conducted using Illumina sequencing data from various tissues, including leaves, stems, flowers, fruits, and roots. RNA-seq alignment files were generated with HISAT2 (v2.1.0),[62] and the PASA pipeline (v2.5.3)[63] was used to align spliced transcripts and annotate candidate genes.

Finally, EVidenceModeler (v2.1.0)[64] was employed to combine the gene models from all approaches. After the initial prediction, PASA was used for three rounds to update the GFF3 file and incorporate alternatively spliced isoforms into the gene models. Telomeres and centromeres in the ZK3-T2T assembly were detected using the software quarTeT (v1.1.5).[65]

Genomic collinearity

Macro-level collinearity analysis was conducted using the JCVI toolkit (Python version of MCScan) (v1.4.23).[66] Genome orientations were manually corrected using SeqKit (v2.8.2)[67] and LiftOn (v1.0.4).[68] Plots were generated using JCVI with default parameters. The locations of inversions were determined based on the output of the simple file.

ChIP-seq analysis

ChIP-seq was performed as previously described.[101] Total proteins were extracted from ZK3 seedlings using lysis buffer (50 mM Tris-HCl, pH 7.5; 150 mM NaCl; 0.1% Triton X-100; 0.2% Nonidet P-40; 1 mM PMSF; 1× protease inhibitor cocktail) and incubated on ice for 30 min. The lysate was centrifuged at 12,000 rpm for 30 min at 4 °C. The protein extract was incubated with either a CENH3 (Abcam) antibody or IgG (as a negative control) (Sigma-Aldrich) at 4 °C overnight. DynaGreen™ Protein A/G beads (Invitrogen) were then added and incubated at 4 °C for 2 h, followed by 4–5 washes with lysis buffer to remove non-specifically bound proteins. An appropriate amount of 2× SDS loading buffer was added, and the samples were boiled for 10 min. The proteins were separated by SDS-PAGE and detected using the CENH3 antibody.

Please cite this article in press as: Zhang et al., Pangenome-guided breeding restores high-altitude adaptation and improves yield in Tartary buckwheat, Cell (2026), https://doi.org/10.1016/j.cell.2026.07.035

Seedlings of ZK3 were cross-linked in MC buffer (10 mM sodium phosphate, pH 7.0, 50 mM NaCl, and 0.1 M sucrose) on ice under vacuum with 1% formaldehyde. Three to five grams of fixed tissue were ground into a fine powder in liquid nitrogen for nuclear isolation. Chromatin was then resuspended in sonication buffer (10 mM sodium phosphate, pH 7.0, 0.1 M NaCl, 0.5% Sarkosyl, 10 mM EDTA, 1× complete protease inhibitor cocktail) and sonicated using a Bioruptor® (Diagenode) to a fragment size of 300 to 500 bp. Anti-CENH3 and IgG control antibodies were used for immunoprecipitation. The immunoprecipitated protein-DNA complexes were reverse cross-linked with proteinase K (Invitrogen), and DNA was purified using VAHTS DNA Clean Beads (Vazyme). The DNA samples were used to construct libraries with the TruePrep DNA Library Prep Kit V2 for Illumina (Vazyme). Libraries were sequenced on an Illumina NovaSeq platform by Annoroad Gene Technology (Beijing, China).

Raw ChIP-seq reads were quality-checked using FastQC (v0.12.1)[69] and trimmed with Trimmomatic (v0.33)[70] to remove adapters and low-quality bases. Cleaned reads were aligned to the reference genome using Bowtie2 (v2.5.4),[71] and the resulting BAM files were sorted with SAMtools (v1.17).[72] Duplicate reads were marked using GATK (v4.2.2.0)[73] MarkDuplicates to minimize PCR bias. Peaks were identified using MACS3 (v3.0.2)[74] with the following parameters: -f BAMPE –broad –broad-cutoff 0.1, using the control sample for background correction.

Cytological analysis

Fourteen tandem repeat sequences located in the potential centromeric regions of chromosomes 1, 3, 4, 5, and 7 were used for multiple sequence alignment using SnapGene (v4.1.9). They showed high homology with each other but differed in length. Thus, the longest sequence, Chr1TR_00141, was selected to generate 58-nucleotide (nt) k-mers. The resulted k-mers were filtered to discard those with melting temperature (Tm) < 66 °C, GC content <30% or >90%. K-mers with more than five consecutive identical nucleotides were also excluded (e.g. GGGGGG). One of the retained k-mer (AGGCTAGTTAATCACCAGGTTAGTCTATGTACTCA TCTCCTTGTTTATTGTTGAGAGT) was selected as a probe, 5′-end-label with 6-carboxyfluorescein (6-FAM), and synthesized by Sangon Biotech (Shanghai).

FISH analysis was performed according to the methods described previously.[102] Hybridization signals were visualized and captured using an Olympus BX-63 epifluorescence microscope equipped with a Photometrics SenSys DP70 CCD camera (Olympus, Tokyo, Japan).

Genome resequenced

Tartary buckwheat accessions were collected by the National Crop Genebank of China and worldwide buckwheat research groups. For phenotypic measurements, the 994 accessions were grown in Liangshan (Sichuan Province), Danzhou (Hainan Province), Weining (Guizhou Province), and Yuanmou (Yunnan Province) from 2018 to 2021. Three randomly selected plants from each accession in each replicate were assessed, and mature seeds were harvested in mid-July. Methods used for cultivation and phenotype measurement are as previously described.[2] Genomic DNA was used to construct sequencing libraries and re-sequenced using the Illumina NovaSeq 6000 platform. Raw reads in FASTQ files were trimmed to remove low-quality bases and adapters using Trimmomatic (v0.33),[70] based on the manufacturer's adapter sequences. After stringent quality control and removal of low-quality reads, sequence alignment to the ZK3 genome indicated an average depth of 16× for each individual. Next, the clean reads from 994 individuals were mapped to the ZK3 genome using the MEM module in BWA-MEM2 (v2.2.1)[75] with default parameters. SAMtools (v1.17)[72] was employed to convert the mapping results to BAM format and filter out unmapped and non-uniquely mapped reads.

SNP calling was carried out following the best-practice workflow recommended by GATK (v4.2.2.0).[73] In brief, SNPs and indels were called for each sample using the HaplotypeCaller module in GVCF mode with GATK (v4.2.2.0), and a joint genotyping step was performed on the combined gVCF file to generate a unified variant call set across all samples. Filtering parameters were set as QD < 2.0 || MQ < 40.0 || FS > 60.0 || SOR > 3.0 || MQRankSum < -12.5 || ReadPosRankSum < -8.0. Additionally, SNPs that were non-biallelic, had > 10% missing data, < 5× approximate read depth, or <0.05 minor allele frequency were removed, yielding a final dataset of 1,158,912 SNPs for further analysis. The identified SNPs and indels were further annotated using the ANNOVAR tool (v2013-05-20)[76] and classified into the following categories: variants in intergenic regions, within 1 Kb upstream or downstream of transcription start or stop sites, in coding sequences, and in introns.

Annotation of the identified population-based SNPs, indels, and SVs was performed using the ANNOVAR package (v2013-05-20)[76] by referring to the ZK3 genome. The SNPs were classified as follows: exonic regions (overlapping with a coding exon), intronic regions (overlapping with an intron), splicing sites (within 2 bp of a splicing junction), upstream and downstream regions (within a 1 Kb region upstream or downstream of the transcription start site), and intergenic regions. SNPs in exonic regions were further grouped into synonymous (resulting in no amino acid change) and non-synonymous (resulting in amino acid changes, including those causing stop-gain and stop-loss) SNPs. To identify variations in *FtRNH* among accessions of HW group, genome resequencing data from HW group accessions were aligned to the XZ751 genome using the same methods described above.

Population genetic analysis

To resolve the population genetic structure and phylogenetic relationships, a neighbor-joining (NJ) tree was constructed based on pairwise genetic distances using 1,364,845 genome-wide SNPs after linkage disequilibrium (LD) pruning ($r^2 < 0.2$) with PLINK (v1.9).[77] The NJ tree was generated using TreeBest (v1.9.2)[78] and visualized with iTOL.[79] The robustness of each tree topology was assessed using 1,000 bootstrap replicates. Population genetic structure was analyzed using the same SNPs as in the NJ tree with ADMIXTURE

Please cite this article in press as: Zhang et al., Pangenome-guided breeding restores high-altitude adaptation and improves yield in Tartary buckwheat, Cell (2026), https://doi.org/10.1016/j.cell.2026.07.035

(v1.23),[80] where the *K* value was set from 1 to 6. Principal component analysis (PCA) was performed using 1,364,845 SNPs and 51,201 SVs with GCTA (v1.94.1).[81] Population linkage disequilibrium (LD) was estimated as squared allele-frequency correlations (r^2) between pairs of SNP loci and plotted using PopLDdecay (v3.41),[82] with r^2 values expressed as percentages.

Pangenome construction

Core and dispensable gene sets were identified based on gene family clustering. Protein sequences from all accessions were subjected to an all-versus-all homology search using DIAMOND (v2.1.4.158).[83] OrthoFinder (v2.5.5)[84] was then run with default parameters to infer orthologous groups. Gene families shared among all accessions were defined as core gene families; those missing in one accession were defined as softcore; those missing in two or more accessions were defined as dispensable; and those present in only one accession were defined as private gene families. For phylogenetic analysis of each gene family, MUSCLE (v3.7)[85] was used for sequence alignment, and the R package ggtree was used for phylogenetic tree visualization. Conserved domains of the family genes were identified using the PfamScan (https://www.ebi.ac.uk/jdispatcher/).

For gene function annotation, Gene Ontology (GO) term enrichment and KEGG pathway analysis were performed using the clusterProfiler package (v4.8.3).[86] Ka/Ks ratios were calculated for the pangenome dataset across core, softcore, dispensable, and private gene sets using WGDI (v0.6.5).[87]

SV identification and graph-based pangenome construction

The graph-based pangenome was constructed using the methods described previously.[103] In detail, the ZK3 genome was set as the reference genome. Synteny analysis of the 15 genomes with ZK3 was performed *via* whole-genome alignment using MUMmer4 (v4.0.1).[88] Genome alignment was carried out using the NUCmer program (-c 100 –mum -l 50), followed by alignment block filtering using the delta-filter program in one-to-one alignment mode (-i 85 -l 100 -m).

We used the SyRI pipeline (v1.7.1)[89] with default parameters to detect structural variants from the resulting filtered delta files. According to the definitions of sequence variation in SyRI outputs, these variations were classified into three types of SVs: PAVs (presence/absence variations), inversions, and translocations. The CPL, DEL, and DUP/INVDP (loss) variants, along with the ZK3 sequences in HDR, NOTAL, and TDM regions, were converted to absence SVs (relative to ZK3) in an accession. The CPG, INS, and DUP/INVDP (gain) variants, together with the query sequences in HDR, NOTAL, and TDM regions, were converted to presence SVs (relative to ZK3) in an accession. INV variants were regarded as inversion SVs relative to ZK3; TRANS and INVTR variants were both regarded as translocation SVs relative to ZK3 in an accession. Identical-type SVs with continuous or overlapping coordinates on a reference or query assembly were merged into a single SV that spanned the entire region covered by the continuous SVs. For details concerning these definitions, refer to: https://schneebergerlab.github.io/syri/fileformat.html. We used a threshold of $\geq$20 bp for SV identification to capture more indels potentially sharing similar functional impacts. The identified SVs from each sample were then merged using SURVIVOR (v1.0.7)[90] with the following parameters: 1000 1 1 1 0 0. The construct function in the vg toolkit (v1.53.0)[91] was used to build the graph-based pangenome by integrating all SVs into the reference genome ZK3-T2T. To genotype structural variations in the 994 accessions, Illumina short reads from each accession were mapped to the graph-based pangenome using the vg toolkit with the map and call functions under default parameters.

SV genomic feature annotation

Throughout the manuscript, we describe various relationships between SVs and other genomic features such as genes. Generally, we annotated our pan-SV genome with genomic features using the ANNOVAR package (v2013-05-20).[76] We define an ''annotation'' as the association of a particular SV with specific feature IDs (e.g., a gene ID) based on a defined genomic relationship. Accordingly, some of the annotations reported in the manuscript can be directly interpreted from ANNOVAR output, such as ''insertions in exons'' or ''deletions overlapping 1 Kb upstream'', as these result directly from feature intersection. Other annotations, such as SVs containing entire genes, required additional intersection-based calculations. For example, to identify genes fully contained within an SV, we first checked whether both the start and end positions of a gene intersected the same SV. If so, the SV was considered to contain that gene. We ultimately produced multiple SV-feature annotation classes, which are described in more detail here. In any applicable annotation, ''upstream'' and ''downstream'' refer to the 5′ or 3′ flanking regions of genes, respectively. In the supplemental material, these ''upstream'' and ''downstream'' regions may also be referred to as ''5′ flanking'' and ''3′ flanking'', respectively.

Pan-graph SV validation

To assess the reliability of pangenomic SVs, eight SVs from different chromosomes were randomly selected for PCR validation in 80 Tartary buckwheat accessions (Primers are listed in Table S5A). The resulting PCR products were aligned to the reference genome for verification.

Selective sweep identification

To detect genomic selective sweeps and genetic differentiation among subpopulations, 1,364,845 population SNPs aligned to the ZK3-T2T reference genome, and 51,201 SVs aligned to the pan-graph reference were used in the following analyses. The cross-population composite likelihood ratio (XP-CLR) test was performed using XP-CLR (v1.1).[92] Genomic regions with XP-CLR values in the top 5% were considered selected regions.

Phylogenetic analysis of genes

The RNH gene family members were identified using OrthoFinder to cluster proteome sequences into orthologous groups. The orthogroup containing FtRNH proteins was selected, and sequences were screened for the presence of the Ribonuclease H domain using InterProScan.[93] To ensure data quality, sequences shorter than 100 amino acids were filtered out.

The extracted RNH domain sequences were aligned using MAFFT (v7.520)[94] with the –auto strategy, which automatically selects the appropriate alignment algorithm based on data size. The resulting alignment was trimmed to remove poorly aligned regions using trimAl (v1.4.rev15)[95] with the -automated1 heuristic method.

Maximum-likelihood (ML) phylogenetic reconstruction was performed using IQ-TREE (v2.2.2.3).[96] The best-fit substitution model was automatically selected by ModelFinder[104] (-m MFP) based on the Bayesian Information Criterion (BIC). Branch support values were calculated using 1,000 ultrafast bootstrap replicates[105] (-bb 1000), with the -bnni option applied to reduce the risk of overestimating branch supports due to model violations. The final phylogenetic tree was visualized and annotated using iTOL (Interactive Tree Of Life).

For other genes, the sequences used for phylogenetic analysis were obtained from Ensembl Plants (http://plants.ensembl.org/index.html) using amino acid sequences as queries. The phylogenetic tree was constructed in MEGA X (v6) using the neighbor-joining method with the JTT substitution model, ''Number of Differences'' as the distance model (default setting in MEGA X), and 1,000 bootstrap replicates.

Genome-wide association study (GWAS)

Genome-wide association studies (GWAS) of yield-associated agronomic traits were performed using the mixed linear model (MLM) implemented in the genome-wide efficient mixed-model association (GEMMA, v0.96)[97] software. After applying filters of MAF $\geq$ 0.01 and missing rate $\leq$ 0.1, a total of 4,820,622 SNPs and 51,201 non-redundant SVs from 994 individuals were used for SNP- and SV-based GWAS, respectively. The following equation was used in the MLM analysis: '$Y = X\alpha + S\beta + K\mu + E$', where Y represents the phenotype; X, the genotype matrix; S, the population structure matrix; and K, the relative kinship matrix. The terms $X\alpha$ and $S\beta$ represent fixed effects, $K\mu$ represents a random effect, and E represents the random residual. The first three principal components (PCs) derived from whole-genome SNPs were used as fixed effects (i.e., the matrix) to correct for population structure, and a kinship matrix based on simple matching coefficients was used for the matrix. Manhattan plots and quantile-quantile (Q-Q) plots of the GWAS results were generated using the CMplot package in R (v4.3.0).

Transgenic materials construction

Total RNA from Tartary buckwheat and *Arabidopsis* seedlings were extracted using the Polysaccharide and Polyphenol Plant Total RNA Extraction Kit (DP441; Tiangen, Beijing, China) according to the manufacturer's protocol. First-strand cDNA was synthesized using HiScript III RT SuperMix for RT-qPCR (R323-01; Vazyme, Nanjing, China) following the manufacturer's instructions. The coding sequences of *FtRNH* and *FtPLATZ3* were amplified with specific primers using cDNA from Tartary buckwheat leaves as the template and cloned.

Tartary buckwheat overexpression and CRISPR-Cas9 lines were constructed using methods described previously.[106] For the CRISPR-Cas9 system, sgRNA sequences were designed using CRISPR Primer Designer (v1.1.2) and cloned into the sgRNA-Cas9 expression vector, which was then introduced into Tartary buckwheat *via Agrobacterium tumefaciens*-mediated transformation.

For *FtRNH*- or *FtPLATZ3*-overexpressing *Arabidopsis*, the *FtRNH*-pCAMBIA1307 or *FtPLATZ3*-pCAMBIA1307 vector plasmid was transformed into *Agrobacterium* strain GV3101.[107] T_0 seeds from lines overexpressing *FtRNH* or *FtPLATZ3* were screened on MS solid medium containing 30 μg/mL hygromycin B, and transgenic *Arabidopsis* plants were verified by PCR or RT-qPCR. T_2 homozygous overexpression lines of *FtRNH* or *FtPLATZ3* were used for subsequent experiments.

For *FtRNH*- and *FtPLATZ3*-overexpressing rice, the coding regions of *FtRNH* and *FtPLATZ3* were inserted into the pCAMBIA1301UbiNOS vector. All recombinant constructs were introduced into rice (Oryza sativa cv. ZH11) *via Agrobacterium tumefaciens*-mediated transformation by a commercial service (Wuhan Biorun Biotechnology Co., Ltd.).[108]

Development of NILs

For NIL-*FtRNH*^{Hap1} or NIL-*FtRNH*^{Hap2} development, high-altitude wild accessions XZ751 (*FtRNH*-Hap1) or XZ625 (*FtRNH*-Hap2) were used as donors and were crossed with the recurrent parent low-altitude landrace ZK3, respectively. The resultant F_1 plants were backcrossed to ZK3. Plants carrying the *FtRNH* gene were selected using molecular marker and subjected to five additional rounds of backcrosses with ZK3. Heterozygous individuals were then self-pollinated to generate homozygous NIL-*FtRNH*^{Hap1} or NIL-*FtRNH*^{Hap2}.

For NIL-*FtPLATZ3*^{Hap2} development, recurrent parent ZK3 (*FtPLATZ3*-Hap1) was crossed with the donor parent HB91 (*FtPLATZ3*-Hap2), and the resultant F_1 plants were backcrossed to ZK3. Plants harboring a 28-bp insertion in the *FtPLATZ3* promoter were selected using a molecular marker and subjected to five additional rounds of backcrossing with ZK3. Heterozygous individuals were then self-pollinated to generate homozygous NIL-*FtPLATZ3*^{Hap2}.

Please cite this article in press as: Zhang et al., Pangenome-guided breeding restores high-altitude adaptation and improves yield in Tartary buckwheat, Cell (2026), https://doi.org/10.1016/j.cell.2026.07.035

For NIL-*FtRNH*^{Hap2}-*FtPLATZ3*^{Hap2} development, NIL-*FtRNH*^{Hap2} and NIL-*FtPLATZ3*^{Hap2} (both in the ZK3 background) were hybridized, and the resultant F_1 plants were self-crossed. Homozygous F_2 plants carrying both *FtRNH*-Hap2 and *FtPLATZ3*-Hap2 alleles were selected as NIL-*FtRNH*^{Hap2}-*FtPLATZ3*^{Hap2}.

For NIL-*FtRNH*^{Hap2}-*FtPLATZ3*^{Hap2}-MC development, NIL-*FtRNH*^{Hap2}-*FtPLATZ3*^{Hap2} plants with more *FtPLATZ* copies were hybridized with the high-altitude buckwheat accession XZ625, which carries few *FtPLATZ* copies. The F_1 plants were then self-crossed to produce an F_2 population. Starting from F_2, individuals with further increased copy numbers (*via* unequal recombination, when available) or mixed-copy individuals were selected and self-crossed. Plants with further increased copy numbers were finally obtained in the F_6 generation. F_6 individuals with further more *FtPLATZ* copies were selected and backcrossed to NIL-*FtRNH*^{Hap2}-*FtPLATZ3*^{Hap2}.

Plants carrying more *FtPLATZ* copies were selected and subjected to five additional rounds of backcrossing with NIL-*FtRNH*^{Hap2}-*FtPLATZ3*^{Hap2}. Heterozygous individuals were then self-pollinated to generate homozygous NIL-*FtRNH*^{Hap2}-*FtPLATZ3*^{Hap2}-MC.

Plant stress treatments and phenotypic assays

Three-week-old *Arabidopsis* seedlings, four-week-old Tartary buckwheat and rice seedlings were used for stress treatments. For UV-B treatment, seedlings were irradiated using Philips TL20W/01 narrow-band UV-B tubes (emission peak ~311 nm) following the methods described previously.[109] To obtain spectrally defined UV-B, the light was filtered using a cellulose diacetate film to remove potential UV-C wavelengths. The UV-B irradiance at the seedling level was maintained at 3.64 W m^{-2}, as measured using a UV irradiance meter (UV340B, Xinbao Scientific Instrument, China). For cold treatment, seedlings were placed in a growth chamber set to 4 °C. For combined UV-B and cold treatment, seedlings were simultaneously subjected to the afore-mentioned UV-B irradiation at 4 °C. Cold stress phenotypic comparison between wild and landrace, and tests with overexpression/mutants were performed in Liangshan, all other cold and UV-B experiments were in Beijing. For phenotypic observation, seedlings were subjected to specified stress for 2 days, then transferred to normal conditions for a 2-day recovery period–during which stress-induced phenotypes became more distinct–before observation. For molecular and biochemical analyses, seedlings were subjected to specified stress for 1 day, followed by a 2-day recovery under normal conditions. Gene expression and transcriptome profiling were assessed immediately after the stress treatment to capture transient stress-responsive transcriptional changes. CPDs and 6-4PPs photoproducts and R-loops were quantified both immediately after stress and after the 2-day recovery period to determine whether the stress conditions indeed induce these lesions and whether the gene functions in preventing damage formation or facilitating post-stress repair. All other analyses, including TUNEL assay, γ-H2AX detection, flavonoid content and the comet assay, were performed exclusively after the 2-day recovery period to allow clearer observation of stress-induced differences. Flavonoid content was measured according to methods described previously.[2,3,16] To observe growth status at different altitudes, Tartary buckwheat seeds were sown in the same soil and then placed at test stations at different altitudes (2,100 m, 2,950 m, and 3,500 m) within the same ecological region.

Quantitative RT-PCR and RNA-seq

Quantitative RT-PCR was performed using the LightCycler 480 Real-Time PCR System (Roche, South San Francisco, CA, USA). The $2^{-\Delta\Delta Ct}$ method and the housekeeping gene *FtACTIN* (*ZK3008232*) were used to normalize transcript levels and calculate the relative expression of target genes. Primer sequences are listed in Table S5A. Total RNA from Tartary buckwheat seedlings was extracted using a Polysaccharide and Polyphenol Plant Total RNA Extraction Kit (TIANGEN) according to the manufacturer's instructions. The RNA samples were used for standard Illumina library construction and sequencing by Annoroad Gene Technology. For bioinformatic analysis, raw sequencing data were quality-controlled using fastp (v1.1.0)[98] to remove adapters and low-quality reads. The resulting clean reads were aligned to the reference genome using HISAT2 (v2.1.0). Gene expression levels were quantified using featureCounts (v2.0.3),[99] and differential expression analysis was performed using the DESeq2 (v1.38.3)[100] package in R software. Genes with an adjusted *P*-value (padj) < 0.05 and an absolute log2 fold change (|log2FC|) > 1 were identified as differentially expressed genes (DEGs).

Dual-luciferase reporter assay

Dual-luciferase assays were performed in *Nicotiana benthamiana via* agroinfiltration. Promoter fragments of *FtPLATZ3* (Hap1, Hap2, Hap2–28bp, Hap1+28bp, Hap2MYB/Dof mutant) and target genes *FtCYC/FtEXP1* were cloned into pGreenII 0800-LUC. The *FtPLATZ3* CDS was constructed into pGreenII 62SK (35S promoter) as effector, with empty 62SK as control. *Agrobacterium tumefaciens* GV3101 (pSoup-p19) harboring constructs was infiltrated at OD_{600} = 0.6–0.8. Following 24 h dark and 48 h light culture, luciferase signals were detected with an LB983 Nightowl II imager after 1 mM potassium luciferin treatment. Primer sequences are listed in Table S5A.

Enzyme activity analysis

For FtRNH enzyme activity assay, single-stranded DNA (ssDNA) and RNA (ssRNA) sequences were generated by ChatGPT-4 as follows: DNA1: TAGCATCGATCACGTACGAT; DNA2: AGCTGCATCGTACGCGTACC; DNA3: GATCGATCACGTACGATCGG. RNA1: AUCGUACGUGAUCGAUGCUA; RNA2: GGUACGCGUACGAUGCAGCU; RNA3: CCGAUCGUACGUGAUCGAUC. In addition,

Please cite this article in press as: Zhang et al., Pangenome-guided breeding restores high-altitude adaptation and improves yield in Tartary buckwheat, Cell (2026), https://doi.org/10.1016/j.cell.2026.07.035

FtPOD DNA: GGCTTGTCCTGGAGTAGTCT; *FtF3'H* DNA: GCAGTCCGTGACGAGGCGGC; *FtPOD* RNA: AGACUACUCCAGGA CAAGCC and *FtF3'H* RNA: GCCGCCUCGUCACGGACUGC were designed based on the results of DRIP-seq. All oligonucleotides were synthesized by Sangon Biotech.

Equimolar amounts of complementary DNA and RNA strands were mixed, denatured at 95°C, and annealed using a temperature gradient to form DNA-RNA hybrids. Recombinant FtRNH-His proteins (including two haplotypes and mutant proteins) were expressed and purified from a prokaryotic system. Meanwhile, empty His-tagged protein was purified and used as a uniform control for all experiments.

For agarose gel electrophoresis analysis, recombinant FtRNH-His protein was serially diluted to final concentrations of 5, 1, 0.5 and 0.25 μM, with empty His-tagged protein as the control. The diluted FtRNH-His proteins at different concentrations were incubated with 10 mM DNA-RNA hybrid substrate in reaction buffer (10 mM Tris, 1 mM $MgCl_2$, pH 7.8) at 37°C for 70 min. Proteins were removed using a commercial StarPrep Gel Extraction Kit (D205, Genstar, Beijing), and the remaining nucleic acids were analyzed by 4% agarose gel electrophoresis. Hybrids exhibited slower electrophoretic mobility than single-stranded nucleic acids due to their larger molecular weight.

For absorbance at 260 nm assay, 5 μM FtRNH-His protein (final concentration) and 10 mM DNA–RNA hybrid substrates were added to the abovementioned reaction buffer, and then incubated at 37°C for 70 min. After removing proteins using abovementioned nucleic acid purification kit, absorbance was measured using a NanoDrop spectrophotometer. The degradation efficiency of FtRNH on R-loops was quantified according to the change in absorbance, an increase in absorbance indicated that the hybrids were degraded into single-stranded nucleic acids.

For the enzymatic kinetic assay, reactions were performed in a 100 μL reaction buffer containing 5 μM FtRNH protein (Hap1 and Hap2, final concentration) and a series of different concentrations of fluorescently labeled DNA-RNA2 substrate, in which DNA strands were labeled with a 6-FAM fluorophore at the 5′ end, and RNA strands were labeled with a Dabcyl quencher at the 3′ end. The reaction was initiated at 37°C, and the fluorescence change of the product was monitored in real-time using a multimode microplate reader (excitation: 488 nm; emission: 520 nm) to detect the product formation rate after removing proteins using abovementioned nucleic acid purification kit. Initial reaction rates were calculated based on the linear range of fluorescence changes. Michaelis-Menten kinetic parameters were determined by nonlinear regression analysis of initial velocity data. Curve fitting was performed using GraphPad Prism 8.0.

Antioxidant enzyme activity assays were conducted using methods described previously.[110]

R-loop level assay

To preserve R-loop levels, genomic DNA was extracted from different plant materials following a previously described protocol.[111] DNA samples were spotted onto a positively charged nylon membrane (Hybond-N+, GE Healthcare) using a dot-blot apparatus. To immobilize nucleic acids, membranes were baked at 80°C for 2 hours. Following fixation, membranes were blocked with 5% (w/v) non-fat milk in TBST buffer. The membrane was incubated with the anti-RNA:DNA hybrid monoclonal antibody S9.6 (1:1000 dilution; MABE1095, Sigma-Aldrich, USA) for 1 hour at room temperature. Subsequently, the membrane was washed and incubated with an HRP-conjugated Goat Anti-Mouse IgG secondary antibody (1:3000 dilution; CW0102S, Cwbiotech, China). Immunoreactive signals were visualized using an Enhanced Chemiluminescence (ECL) substrate and subjected to densitometric analysis.

DRIP-seq

Seedlings subjected to UV-B treatments were used for nuclear extraction. The extracted nuclei were incubated with proteinase K/SDS lysis buffer (0.5 mg proteinase K, 1% SDS, 50 mM Tris-HCl pH 8.0, 20 mM EDTA, and 100 mM NaCl) at 37 °C overnight for genomic DNA extraction. The DNA was fragmented to 200–500 bp by enzymatic digestion (Yeasen Hieff® Smearase). Approximately 5 μg of DNA was incubated with 3 μL S9.6 antibody at 4 °C overnight, followed by the addition of 25 μL DynaGreen™ Protein A/G beads (Invitrogen) and incubation at 4 °C for 2 h for immunoprecipitation. The immunoprecipitated DNA fragments were released from the antibody by proteinase K treatment and then purified by phenol/chloroform extraction and ethanol precipitation. Finally, the purified DNA was used for library construction with the TruePrep RNA Library Prep Kit for Illumina (Vazyme) and subjected to 150-bp paired-end sequencing on an Illumina NovaSeq X Plus platform at Berry Genomics.

CPDs and 6-4PPs content measurement

Genomic DNA was isolated from harvested tissues using the CTAB method. The levels of CPDs and 6-4PPs were determined using the OxiSelect™ UV-Induced DNA Damage ELISA Kits (Cell Biolabs, San Diego, CA), according to the manufacturer's instructions. Briefly, extracted DNA was denatured by heating at 95°C for 10 min and rapidly chilled on ice for 10 min. The denatured DNA was diluted to 2 μg/mL in cold PBS, and 100 μL of the sample was added to the DNA binding plate (provided in the kit) and incubated overnight at 4°C. After blocking, the plates were incubated with anti-CPDs or anti-6-4PPs primary antibodies for 1 h at room temperature, followed by incubation with HRP-conjugated secondary antibodies. The absorbance was measured at 450 nm using a microplate reader. The relative amounts of CPDs and 6-4PPs were calculated based on the standard curves provided by the kits.

Please cite this article in press as: Zhang et al., Pangenome-guided breeding restores high-altitude adaptation and improves yield in Tartary buckwheat, Cell (2026), https://doi.org/10.1016/j.cell.2026.07.035

Comet assay

The method was adapted from previous research[112] with some modifications. Corresponding samples (80 mg), both before and after treatment, were excised with a sharp blade and placed in cold PBS buffer. The samples were thoroughly homogenized using a glass homogenizer, and nuclei were extracted by centrifugation at 12,000 rpm. Subsequently, 100 μl of the supernatant was mixed with 500 μl of 0.5% agarose (Amresco, USA) at 4 °C. The mixture was immediately pipetted onto a microscope slide and cooled on ice for 1 minute.

The slides were then immersed in lysis buffer (2.5% w/v SDS in 0.5% TBE buffer) for 1 hour, followed by electrophoresis at 15 V for 20 minutes. The slides were stained with 1 μg/mL propidium iodide (PI) for 10 minutes and observed under a fluorescence microscope BX61 (Olympus). The Comet Analysis Software Project (CASP) was used to evaluate comets from 30 nuclei per sample. The percentage of cellular DNA that migrated into the comet tail (tail DNA content) was used to assess the extent of DNA damage.

γ-H2AX immunofluorescence assay

DNA double-strand breaks were visualized *via* immunofluorescence staining of γ-H2AX. Paraffin-embedded sections were deparaffinized, rehydrated, and subjected to heat-induced antigen retrieval in citrate buffer. After blocking with 3% BSA for 30 min at room temperature, the sections were incubated with an anti-γ-H2AX primary antibody (Millipore, 05–636) overnight at 4°C. Subsequently, the sections were incubated with an Alexa Fluor™ 488-conjugated secondary antibody (1:2,000) for 50 min at room temperature in the dark. Nuclei were counterstained with PI (Propidium Iodide) for 10 min. To minimize background interference, an autofluorescence quencher was applied for 5 min before mounting. Images were captured using a fluorescence microscope, with γ-H2AX-positive signals identified as green fluorescent foci within the nuclei.

TUNEL staining

Cell death in plant tissues was detected using a TUNEL fluorescence assay kit (TMR-red). Paraffin-embedded sections were deparaffinized, rehydrated, and incubated with Proteinase K (20 μg/mL) at 37°C for 20 min for antigen retrieval. The sections were then incubated with the TUNEL reaction mixture (containing TdT enzyme and dUTP) in a humidified chamber at 37°C for 1 h in the dark. Nuclei were counterstained with DAPI. Images were captured using a fluorescence microscope: apoptotic cells exhibited red fluorescence (TMR, Ex/Em = 510–561/590 nm), while nuclei showed blue fluorescence (DAPI, Ex/Em = 330–380/420 nm).

Subcellular localization identification

The full-length CDS of *FtRNH* and *FtPLATZ3* were cloned into the pCAMBIA1300 vector containing the CaMV 35S promoter to drive GFP expression. The recombinant vector and p2300-35S-H2B-mCherry (a nuclear marker) were co-transformed into *Agrobacterium tumefaciens* GV3101. Following transient expression of the FtPLATZ3-GFP fusion protein in *N. benthamiana*, subcellular localization was observed using a laser scanning confocal microscope (LSM900, Zeiss). The experiment was repeated three times using different leaves of *N. benthamiana*, yielding consistent results. Primer sequences are listed in Table S5A.

Paraffin sectioning

Immature kernels were collected and immediately fixed in FAA solution (50% ethanol, 10% formaldehyde, and 5% acetic acid, v/v). Vacuum infiltration was applied for 20 min, and the samples were then stored at 4 °C until further processing. The samples were dehydrated through a graded ethanol series, followed by clearing in xylene and embedding in paraffin. Sections of 10 μm thickness were cut using a microtome and stained with 0.1% toluidine blue. The stained sections were mounted with neutral resin and observed under a light microscope.

EMSA

The CDS of *FtPLATZ3* was cloned into the pGEX-4T-1 vector, and the recombinant plasmid was transformed into *Escherichia coli* BL21 (DE3) competent cells. The FtPLATZ3–GST fusion protein and the GST-tag protein (used as a control) were induced with 0.1 mM IPTG at 16 °C when the culture reached an OD_{600} of 0.6 and then purified using GST•Bind™ Resin (Millipore). The purified proteins were subjected to EMSA. Biotin-labeled probes were synthesized by Sangon Biotech. The probes were denatured at 95 °C for 5 min and then slowly cooled to room temperature to allow annealing into double-stranded DNA. EMSA reactions were performed using the LightShift Chemiluminescent EMSA Kit (Thermo Fisher Scientific) according to the manufacturer's instructions.

DAP-seq

Genomic DNA from ZK3 seedlings was used to construct DNA libraries using the TruePrep DNA Library Prep Kit V2 for Illumina (Vazyme). The FtPLATZ3-Halo fusion protein and the empty Halo-tagged protein (as a negative control) were synthesized by *in vitro* translation using the TNT SP6 High-Yield Wheat Germ Protein Expression System (Promega). The proteins were then incubated with HaloTag Beads (Promega) for 2 h, followed by three washes with TBSN buffer (100 mM Tris-HCl, pH 7.5; 50 mM NaCl; 0.005% NP-40). Subsequently, 5 μg of the ZK3 DNA library was added and incubated for 1.5 h, and the beads were washed with TBSN buffer to remove nonspecifically bound DNA. The bound DNA was eluted with ddH_2O and subjected to PCR amplification. PCR products were purified and size-selected using VAHTS DNA Clean Beads (Vazyme) and sequenced by Annoroad Gene Technology.

Please cite this article in press as: Zhang et al., Pangenome-guided breeding restores high-altitude adaptation and improves yield in Tartary buckwheat, Cell (2026), https://doi.org/10.1016/j.cell.2026.07.035

Yeast two-hybrid assay

The CDS fragments of *FtRPC53a* and *FtTFC1* were ligated into the pGBKT7 plasmid. The full-length coding sequence of *FtPLATZ3* was cloned into the pGADT7 AD vector (Clontech, Mountain View, CA, USA). The recombinant AD and BD vectors were co-transformed into the yeast strain Y2HGold. Co-transformants were serially diluted and spotted onto control medium (SD/-Trp/-Leu) and selective medium (SD/-Trp/-Leu/-His/-Ade), and incubated for 4 days.[113] Primer sequences are listed in Table S5A.

Field planting and yield measurement

Field trials were conducted at five elevational sites with three independent experimental plots established at each site. The locations were as follows: Zhaojue County, Sichuan Province (27.9909°N, 102.8402°E; alt. 2100 m); Zhaotong, Yunnan Province (27.4224°N, 103.3013°E; alt. 3060 m); Nyingchi, Xizang Autonomous Region (29.3253°N, 94.3402°E; alt. 2950 m); Lhasa, Xizang Autonomous Region (29.3618°N, 90.7408°E; alt. 3600 m); and Xietongmen County, Rikaze, Xizang Autonomous Region (29.4085°N, 88.1886°E; alt. 3900 m). Seeds were sown at each site when the daily mean temperature stably exceeded 10 °C using drill seeding, with a row spacing of 33 cm and a sowing rate of 6 g/m^2. Field management was performed in accordance with local standard agronomic practices. Phenotypic traits were measured at corresponding developmental stages. Plants were harvested when more than 75% of the seeds reached physiological maturity, and grain yield was adjusted and calculated based on a standardized seed moisture content of 13%. For phenotypic and yield determination, 40 randomly sampled individual plants per genotype from each independent experimental plot were measured and analyzed.

QUANTIFICATION AND STATISTICAL ANALYSIS

Data are presented as means ± standard deviation (SD) or 95% confidence interval (CI) as indicated in the corresponding figure legends. Error bars represent SD or 95% CI. The related environmental factors of accessions are available in Table S3C. The presence and absence of the related genes and haplotypes were recovered from the corresponding genome data. All statistical analyses including Student's *t* test, one-way ANOVA, two-way ANOVA, and subsequent Tukey's HSD post hoc test were performed in R software (v4.2.3). The results of two-way ANOVA are presented in Table S5B.